1-4-95

SANDIA REPORT

SAND94—2578 • UC—900
Unlimited Release
Printed October 1994

Integrated Structural Control Design of Large Space Structures

James J. Allen, James P. Lauffer

Prepared by
Sandia National Laboratories
Albuquerque, New Mexico 87185 and Livermore, California 94550
for the United States Department of Energy
under Contract DE-AC04-94AL85000

Issued by Sandia National Laboratories, operated for the United States Department of Energy by Sandia Corporation.

Available to DOE and DOE contractors from
Office of Scientific and Technical Information
PO Box 62
Oak Ridge, TN 37831

Prices available from (615) 576-8401, FTS 626-8401

Available to the public from
National Technical Information Service
US Department of Commerce
5285 Port Royal Rd
Springfield, VA 22161

NTIS price codes
Printed copy: A04
Microfiche copy: A01

Acknowledgment

This work was performed at Sandia National Laboratories and was supported by the U.S. Department of Energy under Contract Number DE-AC04-94AL85000 via the Laboratory Directed Research and Development program.

Forward

The purpose of this project was to develop expertise in the design and implementation of active structural control techniques for large space structures which is a technical problem of great importance to national objectives in defense and space exploration. Currently much of the technology developed in this area are also finding application in transportation and manufacturing. The project focused on the design, implementation and comparison of techniques for structural system identification and robust structural control design.

The next logical step for the technical community is an actual *space* experiment. As a result of technical interactions brought about by this LDRD with several government agencies, a low cost/low Earth orbit active structural control experiment (LASC) was proposed. This LDRD provided the technical thrust and concept to pursue LASC.

During the last year of the project, work was perform on Single Input/Single Output (SISO) active damping methods which will be reported separately. We also worked with NASA Marshall Space Flight Center in Huntsville, Alabama to implement the identification and control methods investigated under this LDRD on the Control, Astrophysics, and Structures Experiment for Space Ground Test Facility(CASES-GTF); however, this work was not completed due to instrumentation difficulties with the testbed as NASA/Marshall.

Table of Contents

List of Figures

List of Tables

Integrated Structural Control Design of Large Space Structures

Introduction

Active control of structures has been under intensive development for the last ten years. Reference 2 reviews much of the identification and control technology for structural control developed during this time. The technology was initially focused on space structure and weapon applications; however, recently the technology is also being directed toward applications in manufacturing and transportation. Much of this technology focused on multiple-input/multiple-output (MIMO) identification and control methodology because many of the applications require a coordinated control involving multiple disturbances and control objectives where multiple actuators and sensors are necessary for high performance. There have been many optimal robust control methods [1,2] developed for the design of MIMO robust control laws; however, there appears to be a significant gap between the theoretical development and experimental evaluation of control and identification methods to address structural control applications.

Many methods have been developed for MIMO identification and control of structures [2], such as the Eigensystem Realization Algorithm (ERA), Q-Markov Covariance Equivalent Realization (Q-Markov COVER) for identification; and, Linear Quadratic Gaussian (LQG), Frequency Weighted LQG and H_∞/μ-synthesis methods for control. Upon implementation, many of the identification and control methods have shown limitations such as the excitation of unmodelled dynamics and sensitivity to system parameter variations. As a result, research on methods which address these problems [2] have been conducted. All of these identification and control methods are challenged by the characteristics of structural systems and implementation limitations such as:

- High order system dynamics
- High modal density
- Closely coupled dynamics
- Actuator and Sensor limitations
- External unmeasured inputs
- Frequency regimes with low signal to noise
- Limited control processor capabilities

The main purpose of this LDRD project is to assess the capability of identification and control methods for vibration suppression of structural systems. Many identification and control methods have been theoretically developed and extensively analyzed; however, the number of applications of the technology presented in the literature which discuss the experimental implementation details of identification and control design are limited.

Unless the implementation details of these identification and control methods (i.e. data collection and assessment, weight selection and justification, etc.) are thoroughly understood for a variety of applications, many of these methods will not be applied to engineering systems on a regular basis.

The experimental focus of this project is the *Sandia Truss*, which like many structures, represents a challenge to the existing identification and control methods due to a variety of phenomena previously mentioned. Earlier research in designing LQG controllers for the *Sandia Truss* based on a finite element model (FEM) of the system showed sensitivity of LQG controllers to parameter variations [2] and the difficulty of obtaining FEM's with the necessary accuracy for high performance control [3]. Based on this experience, the project focused on the development of control design models from experimental data and robust control methods.

The linear quadratic gaussian (LQG) control method was developed thirty years ago and is capable of designing MIMO control laws. However, LQG controllers designed with white disturbance and sensor noises do not produce satisfactory results [3]. Augmenting the model of the system dynamics with frequency weighting filters for the disturbance, sensor noise and control signal was proposed by Gupta [4] to obtain a frequency weighted LQG (FWLQG) method. The FWLQG method can be used to design loopshaping controllers which gain stabilize unstructured system uncertainty. Safanov [5] also suggested the use of colored noises in LQG design to obtain robustness in the control law. Reference 6 describes the application of FWLQG to a one bay truss structure which had three dominant modes in the performance output and several less significant modes in the system dynamics, which was modeled for control design purposes by the finite element method. The experimental study in reference 6 produced stable but overly conservative control systems which limited the system performance.

Maximum Entropy (ME) is a method of modeling structured parameter uncertainty via a stochastic multiplicative white-noise process. This approach allows the performance/ robustness trade-off to be determined by a quadratic cost function. Maximum Entropy specifically addresses real valued parameter uncertainties which are significant in the design of structural control systems. Maximum Entropy necessary conditions for optimality [7] result in two Riccati and two Lyapunov equations which are coupled by the stochastic parameters. Solutions to the coupled Riccati and Lyapunov equations can be obtained by homotopy methods [8]. Experimental evaluations of decentralized ME controllers are reported in reference 9.

This project explored the use of Frequency Weighted LQG in conjunction with Maximum Entropy for the design of disturbance rejection controllers on an experimental truss structure. The frequency weighting allowed gain stabilization of the system dynamics in frequency ranges where there was unstructured uncertainty due to low signal to noise (SNR) or high uncertainty in the system dynamics (e.g. unmodelled dynamics). Maximum entropy was be used for enhanced robustness of structured uncertainty due to uncertain in-band system dynamics.

μ-synthesis is a control design methodology which has been developed to design controllers which satisfy robust performance and stability requirements [1-16]. μ-synthesis integrates, H_∞ controller synthesis and the structured singular value (μ) control analysis into a systematic design methodology.The basic concepts of μ-synthesis can be explained in the context of a general system interconnection structure of plant dynamics (P), controller (K) and uncertainty (Δ). The objective of the H_∞ control problem is to find a stabilizing controller, K, which minimizes the H_∞ norm of the system performance objectives for the nominal system (Δ=0). State space methods of obtaining these solutions have been developed, and the minimization is done using an iterative scheme (γ iteration). The stability bounds of the system due to the uncertainty Δ can be evaluated using the H_∞ norm and the small gain theorem; however, this approach has been shown to be overly conservative when the uncertainty Δ has structure. To handle limitations of the H_∞ norm measure of uncertainty, the structured singular value, μ has been developed. The structured singular value is a matrix function which assumes that the uncertainty Δ has an underlying structure, which is related to the uncertainty and performance objectives. The problem of μ synthesis control design is to find a stabilizing controller, K, which minimizes the H_∞ norm of the system performance objectives for a system with a structured uncertainty, Δ. D-K iteration is an algorithm capable of accomplishing this task; however, global convergence cannot be guaranteed.

The paper is organized as follows. Section discusses the experimental truss structure and describes the control design problem. Section discussed the experimental system identification which was performed to obtain a control design model for the system. Section will present an overview of the control design methods used in this study; and, section will present the experimental control implementation results. Section will summarize results and offer conclusions.

System Description and Control Design Requirements

To evaluate and demonstrate the effectiveness of the experimental system identification and robust control design techniques, we focused on an experimental program which utilized the Sandia Truss as a controlled structure test bed. A schematic of the truss is shown in Figures 1 and 2. The truss is constructed from 1" diameter polycarbonate tubing bonded to polycarbonate blocks at the truss nodes. The truss is "T" shaped with five vertical bays providing the length and two horizontal bays at the top. Each bay is approximately one foot cube. Bolted to the surfaces of two bays are 0.5" polycarbonate plates stiffened with 0.5" thick ribs. The entire truss is cantilevered from a 2000 lbm. seismic mass which in turn is supported on air bags to isolate the structure from high frequency base vibrations.

Eight feedback sensors are utilized to sense the axial strain in the diagonal struts of the bottom two bays of the truss. The sensors are made of polyvinyldene fluoride (PVDF) and are bonded directly to the tubes. These sensors are capable of detecting strains on the order of 10 nanostrain. Charge amplifiers are used as signal conditioners.

The feedback actuators are constructed out of a piezoelectric ceramic, lead magnesium niobate (PMN). The PMN actuators were fabricated in split rings to allow for the actuators to be applied after the construction of the truss. The PMN actuators apply an axial strain to the strut. They are driven by high gain/bandwidth amplifiers capable of providing the DC offset necessary for the PMN actuators. The use of wide bandwidth amplifiers is a major change from a previous study[10] in which the amplifier bandwidth extended to only 120 Hz. Four actuators are located on the diagonal members of the bottom bay of the truss.

The disturbance actuators are made out of PVDF and are identical to the feedback sensors. They are located on the axial struts of the second bay. Like the feedback actuators, the disturbance actuators apply axial strains to the struts.

The controllers were implemented by a digital controls processor. The processor is capable of implementing a 32 state controller with eight inputs and eight outputs while operating at a fixed sampling rate of 50 kHz. The effective transport delay across the processor, including zero order hold effects, is 35 μseconds. To obtain the minimum delay, the processor implements a block-diagonal state-space form of the controller. The principle limitation of this digital processor is that it is incapable of directly implementing a controller in state space form which requires a through-put matrix. When required, the throughput matrix is approximated by including high-frequency real poles in the state transition matrix.

The performances minimized in this study were the x,y,z accelerations at the center of the plate on the top outboard bay. The performances are directly measured using high sensitivity piezoelectric accelerometers. The performances are used to evaluate the effectiveness of the controllers but are *not* used for control feedback.

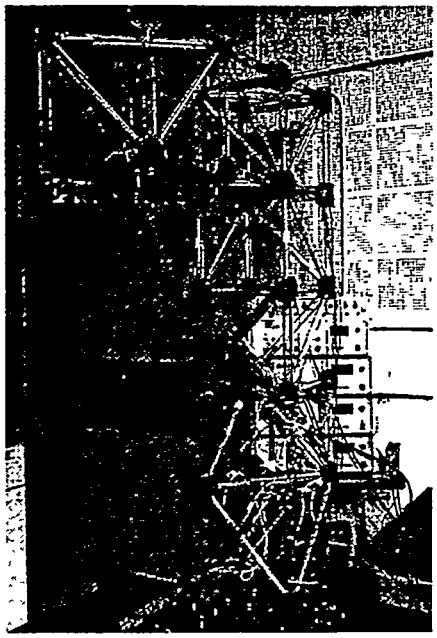

Figure 1. Sandia Truss

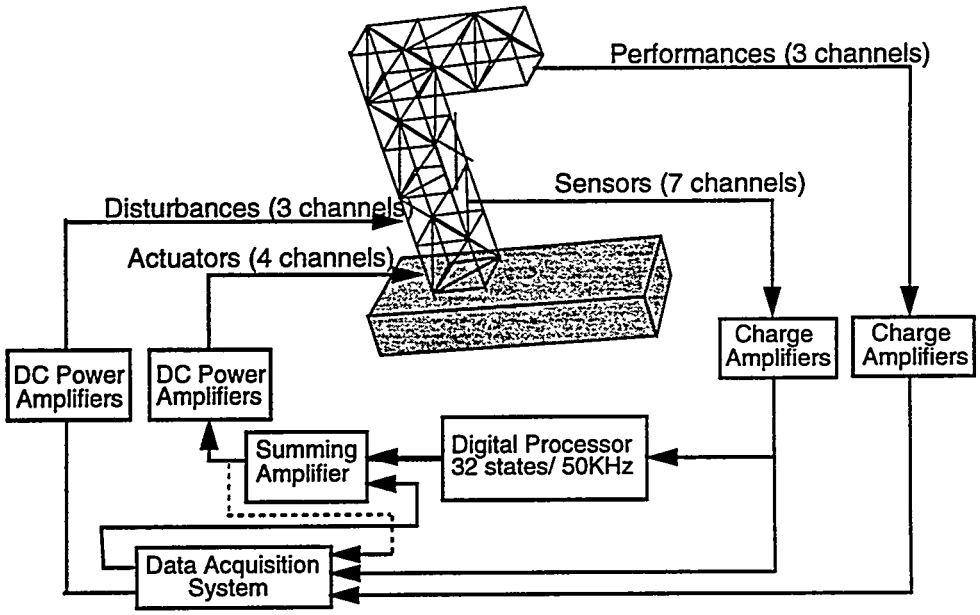

Figure 2. Sandia Truss Instrumentation Diagram

The control design objective for this system can be stated as follows:

- Minimize the elastic response of the system at the performance locations (i.e. x,y,z response of the plate at the top outboard bay) in the frequency range of 10 - 120 Hz, while satisfying the following criteria:
  - Maintain system stability and performance in the face of high frequency uncertain or unmodelled dynamics.
  - Do not excite the low frequency suspension dynamics of the system (<10 Hz) whose dynamics are poorly characterized.

Experimental System Identification

Structural systems provide a significant challenge to system identification algorithms due to high order, high modal density, widely varying damping factors, and multiple inputs and outputs. Finite element models (FEM's) have a great difficulty producing models which are accurate beyond the first few global modes of the system, due to the modelling assumptions that must be made by the analyst, and the inability to apriori model some phenomena (i.e. joint stiffness, damping). Because of the added difficulty of updating FEM's, this study aimed at directly estimating analytical models from test data. The method used for estimating the dynamics of the system was the Eigensystem Realization Algorithm using Data Correlation (ERADC) [11], which extracts a model in a discrete state-space form.

For the system identification experiments, the first objective was to obtain input/output data from which a model could be extracted. ERADC operates on impulse response functions which were estimated by taking the inverse Fourier transforms of frequency response functions (FRF's). In estimating the FRF's, all eight actuators simultaneously excited the truss with uncorrelated burst random excitation. All of the actuator inputs and sensor response signals were simultaneously measured. FRF's were measured over the bandwidth of 0 to 200 Hz with a frequency resolution of 0.125 Hz/spectral line. No weighting windows were applied to the data. Additionally, a second FRF data set was acquired over the bandwidth of 0 to 25 Hz with a resolution of 0.0156 Hz/spectral line. Because of the presence of unmeasured external disturbances and the large number of inputs, an extremely high number of ensemble averages (200) were used in estimating the FRF's. The FRF's were calculated using the H_v[5] estimator.

In the course of estimating FRF's, we also estimated multiple coherence functions [12] and autospectra. These functions were useful in assessing the quality of the measured FRF's and determining the source of errors. Plotted in Figure 3 are a FRF and a multiple coherence function. The FRF is noisy below 15 Hz, which corresponds to the low value of the multiple coherence function over this same frequency range. The noisy estimate of the FRF over this range is due to the low level of response of the structure due to the applied disturbances and the relatively high level response of the suspension modes due to unmeasured floor vibrations. This observation is further substantiated by comparing autospectra of one of the sensors with and without the artificial disturbance activated as shown in, Figure 4. Below 15 Hz, the two autospectra have similar amplitudes which implies that most of the response over this band is due to the unmeasured disturbances.

Due to the noisy estimate of the FRF's over the low frequency band, the resultant models from any system identification technique would be substantially in error over this band. Because of the error in the model and the presence of unmeasured disturbances the low frequency range provides a challenge to the control design.

One of the challenges of employing system identification techniques like ERADC is estimating the order of the system. The principle approach is to select the order by observing the singular values of the system correlation matrix. Ideally, the correct order is

determined from a sudden drop in the magnitude of the singular value plot. Unfortunately, because of the presence of nonlinearities, residual flexibilities, and marginally observable and controllable modes, the system order is seldom readily apparent. The main tool used for order determination in this study was the complex mode indicator function (CMIF) [13].

The CMIF's, which are used extensively in robust control design, are the singular values of the FRF matrix as a function of frequency. The peaks of the CMIF occur at the same frequencies as the system resonances. Multiplicity of roots is indicated by peaks in the secondary and tertiary CMIF's; therefore, the system order can be determined simply by counting the peaks in the CMIF's over the bandwidth of interest. Because of the first order form of the extracted model, the system order is twice the number of peaks in the CMIF's.

In performing ERADC analysis the correlation matrix size is selected to be significantly larger than the estimated system order to account for noise, nonlinearities, etc. System order, length of time records, and matrix size are varied and convergence of parameters is observed. In particular, the eigenvalues of the system should correspond to the peaks in the CMIF, and the damping ratio values should stabilize with increasing matrix size, system order and length of time record. As a single figure of merit to determine the accuracy of a derived model, CMIF's of the measured FRF's and analytical FRF's, calculated from the realized model, can be compared.

System models were estimated in using the ERADC algorithm as coded in the NASA System Identification toolbox [14]. The model was estimated over the frequency range of 0 to 200 Hz. Additional analyses were performed for higher resolution/signal-to-noise analysis band of 0 to 25 Hz. Shown in Figure 5 is a comparison of the CMIF's for the measured and analytical FRF's calculated from the experimentally derived model. The CMIF's are in excellent agreement up to approximately 150 Hz. Above 150 Hz the modal density of the structure is extremely high principally due to local modes of the individual struts. Additionally, the "rigid-body" modes, less than 5 Hz, are not well characterized. The principal reason is that contribution of these modes to the response matrix is a result of external unmeasured inputs and not related to system inputs. These modes are marginally observable and controllable and are poorly characterized by the all of the system identification techniques employed.

The full order system model contained 54 states. Because of instrumentation problems, the final system model consisted of seven inputs (four control actuators and three disturbances) and ten outputs (three performance measures and seven feedback sensors). The dynamics of the truss consist of lightly damped (~0.5%) modes up to (~120 Hz). The structure has a discrete modal *nature* up to ~150 Hz. Above 150 Hz the dynamics become very dense and dominated by many localized modes of the truss. The suspension modes of the isolation mass are at low frequency (~1-3 Hz). The low frequency range also has poor signal to noise characteristics due to the ambient floor vibration.

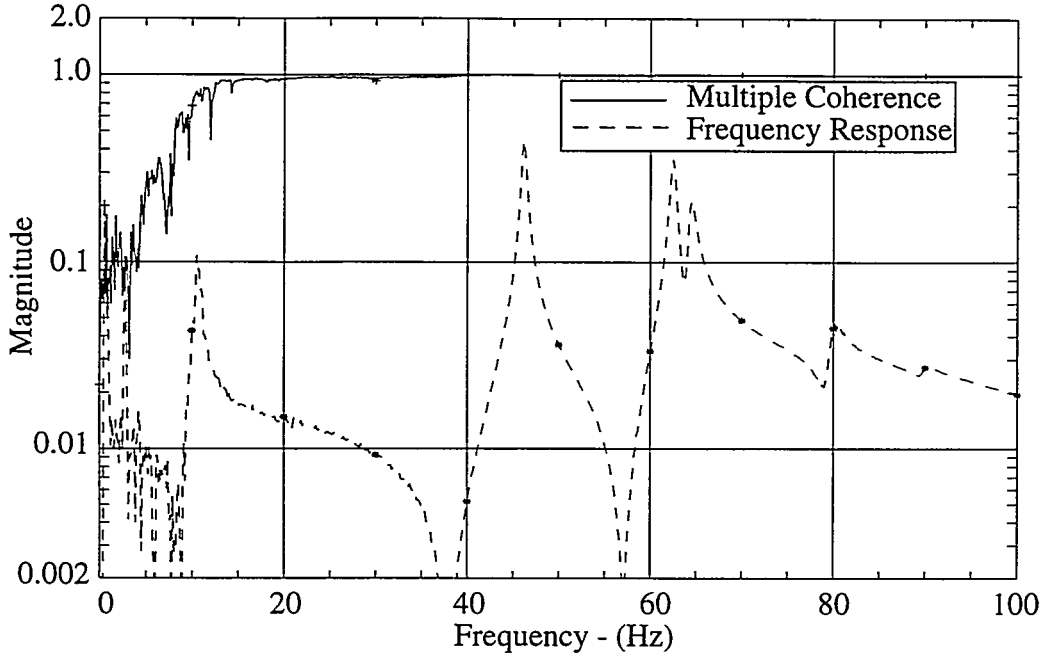

Figure 3. FRF and Multiple Coherence Function

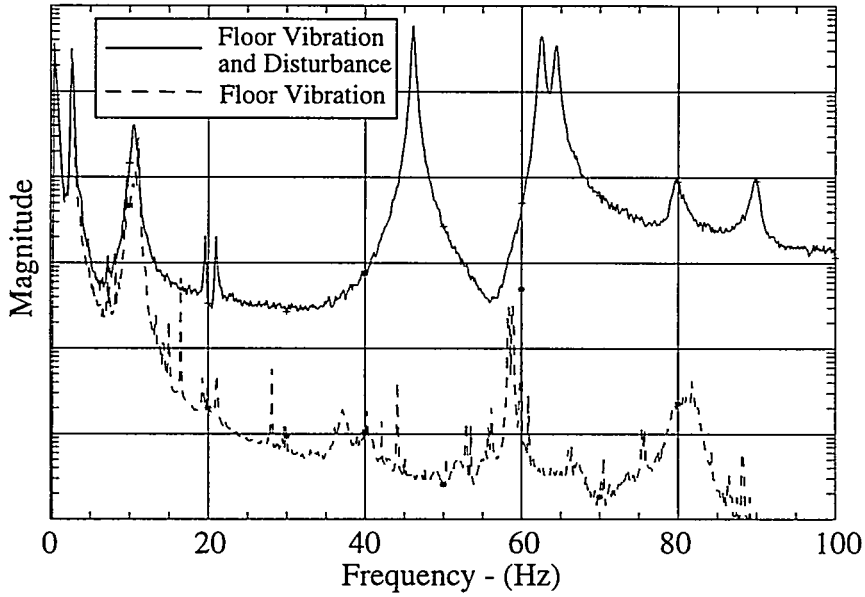

Figure 4. Autospectra with and without Artificial Disturbance.

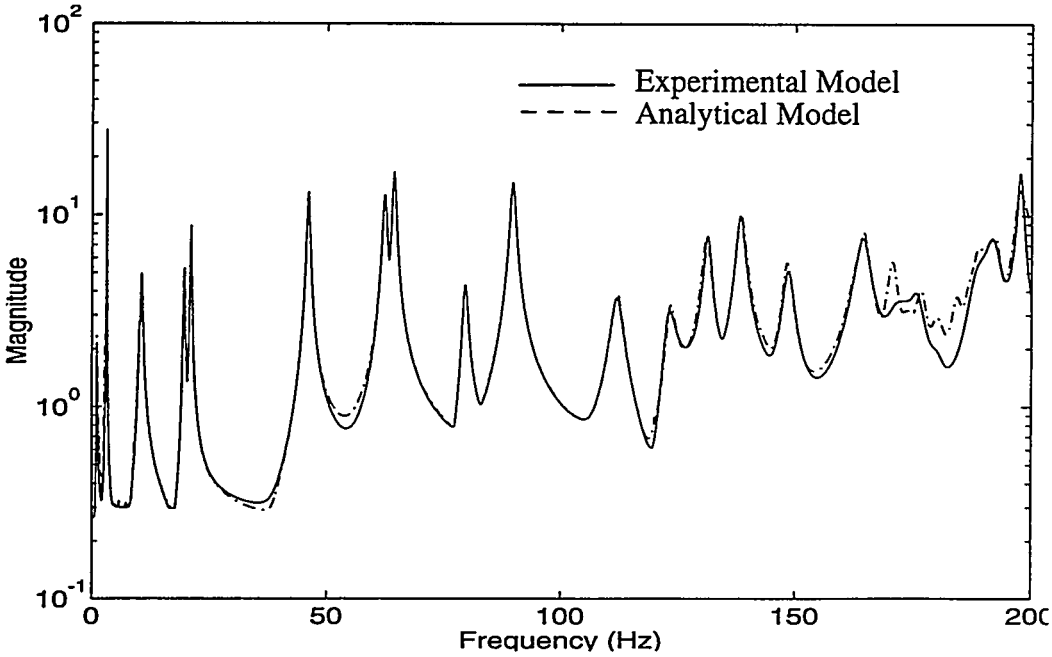

Figure 5. Comparison of CMIF's from measured data and analytical model

Linear Quadratic Control Design Methods

In this section frequency weighted LQG and Maximum Entropy will be reviewed. As a prelude to the discussion of frequency weighted LQG, LQG with cross weighting terms will be reviewed to establish definitions and nomenclature. Only the main results of LQG will be stated, more complete details can be found in reference 1.

LQG Theory:

The problem addressed by LQG theory is the following. Given a system and associated model, figure 6 and equation 1, respectively, design a compensator of the form shown in equation 2, where u,v,w,x, x_c,y,z are the control signal, sensor noise, disturbance, system state, compensator state, performance and sensor vectors, respectively.

$$\begin{aligned} \dot{x} &= \mathbf{A}x + \mathbf{B}_u u + \mathbf{B}_w w \\ y &= \mathbf{C}x + \mathbf{D}_u u + \mathbf{D}_w w \\ z &= \mathbf{M}x + \mathbf{N}_u u + \mathbf{N}_w w + v \end{aligned} \qquad \text{:System Dynamics - } G_0 \qquad \textbf{(1)}$$

$$\begin{aligned} \dot{x}_c &= \mathbf{A}_c x_c + \mathbf{B}_c z \\ u &= \mathbf{C}_c x_c \end{aligned} \qquad \text{:Compensator - K} \qquad \textbf{(2)}$$

The signals w and v are *white* zero-mean gaussian stochastic processes which have the following covariances $E\{ww^T\} = \mathbf{V}_1 \geq 0$ $E\{vv^T\} = \mathbf{V}_2 > 0$ $E\{wv^T\} = \mathbf{V}_{12}$.

The problem is to find a control law which minimizes the cost function shown in equation 3, where $\mathbf{R}_1 = \mathbf{R}_1^T \geq 0$, $\mathbf{R}_2 = \mathbf{R}_2^T > 0$, and $\mathbf{R}_{12}$ are weighting matrices.

$$J = \lim_{T \to \infty} E\{\int_0^T \left(x^T \mathbf{R}_1 x + u^T \mathbf{R}_2 u + 2y^T \mathbf{R}_{12} u \right) dt\} \qquad \textbf{(3)}$$

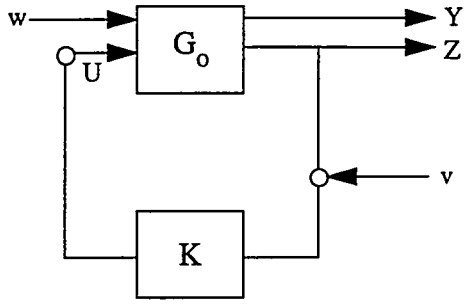

Figure 6. System Schematic

The solution to the LQG problem is prescribed by the **separation principle**, which solves the problem in two uncoupled steps.

- Obtain an optimal estimate, $\hat{x}$, of the state x such that $E\{(x-\hat{x})^T(x-\hat{x})\}$ is minimized. The solution to this problem is given by Kalman filter theory (LQE).
- Use the state estimate, $\hat{x}$, as if it were an exact measurement of the state to solve the deterministic linear quadratic regulator (LQR) problem.

The solution to the LQE and LQR problems each involve the solution of an algebraic Riccati equation. The Kalman-filter gain matrix F is given by equation 4 in which **Q** is the solution of the Riccati equation 5, where $\bar{A} = A - B_w V_{12} V_2^{-1} M$ and $\bar{V}_1 = V_1 - V_{12} V_2^{-1} V_{12}^T$.

$$\mathbf{F} = \left(\mathbf{B_w V_{12}} + \mathbf{Q M^T}\right)\mathbf{V_2}^{-1} \qquad \text{:LQE Gain} \qquad \textbf{(4)}$$

$$\mathbf{Q\bar{A}^T} + \mathbf{\bar{A}Q} - \mathbf{Q M^T V_2^{-1} M Q} + \mathbf{B_w \bar{V}_1 B_w^T} = 0 \qquad \text{: LQE Riccati} \qquad \textbf{(5)}$$

The optimal state feedback matrix, G, of the LQR problem is given by equations 6 and 5, where, $\tilde{A} = A - B_u R_2^{-1} R_{12}^T$ and $\tilde{R}_1 = R_1 - R_{12} R_2^{-1} R_{12}^T$.

$$\mathbf{G} = -\mathbf{R_2^{-1}}\left(\mathbf{R_{12}^T} + \mathbf{B_u^T P}\right) \qquad \text{:LQR Gain} \qquad \textbf{(6)}$$

$$\tilde{\mathbf{A}}^{\mathbf{T}}\mathbf{P} + \mathbf{P}\tilde{\mathbf{A}} - \mathbf{P B_u R_2^{-1} B_u^T P} + \tilde{\mathbf{R}}_1 = 0 \qquad \text{:LQR Riccati} \qquad \textbf{(7)}$$

The matrices for the compensator designed by the LQG procedure which is of the form shown in equation 2 are given in equation 8.

$$A_c = A + B_u G - F(M + N_u G)$$
$$B_c = FM \qquad (8)$$
$$C_c = G$$

The LQG development is based on optimization methods with a specified model form. The closed loop system behaves well under the following conditions

- The model is valid for all values of inputs and states and the dynamics are well described at all frequencies.
- The Kalman filter design also assumes that the dynamics are known equally well at all frequencies. This may also make combination of the Kalman filter and the LQR control law extremely sensitive to errors.
- The optimality of the Kalman filter is strongly dependent on the accuracy of the noise statistics.

The experience with LQG controllers designed with white noises have not been completely satisfactory [3]. In addition there are no explicit ways in the technique presented above to design a controller with a specified bandwidth or stability margins.

Frequency Weighted LQG Theory:

An effort to correct some of the problems associated with LQG theory have been implemented through the use of colored noises and frequency dependent weighting in LQG formulation. In reference 4, Gupta presented a method of incorporating frequency dependent cost functions into basic LQG theory. A formulation for Frequency Weighted LQG (FWLQG) which incorporates the methods presented in references 4, 5 and 6 is presented here.

Figure 7 shows a schematic of a system which has a control signal weighting filter, G_u and noise coloring filters G_d and G_s appended. G_0 and K are as defined previously. The state space matrices corresponding to the weighting and coloring filters are defined below.

G_u - Control Weighting Filter: $\begin{bmatrix} A_\mu & B_\mu \\ C_\mu & D_\mu \end{bmatrix}$

G_s - Sensor Noise Coloring Filter: $\begin{bmatrix} A_s & B_s \\ C_s & D_s \end{bmatrix}$

G_d - Disturbance Noise Coloring Filter: $\begin{bmatrix} A_d & B_d \\ C_d & D_d \end{bmatrix}$

The rationale behind the definition of inputs and weightings are as follows.

- The external disturbance that the control system is to reject is the white noise disturbance w colored by G_d.

- The *white noise* disturbance w_d is used to enhance stability margin at the input. The intensity of this noise can be physically interpreted as uncertainty in the actuator.
- The measurement noise v is colored by G_s to simulate physical sensor noise or possible model uncertainty.
- The filtered control signal, μ, can be used to penalize control effort outside the frequency range of interest.

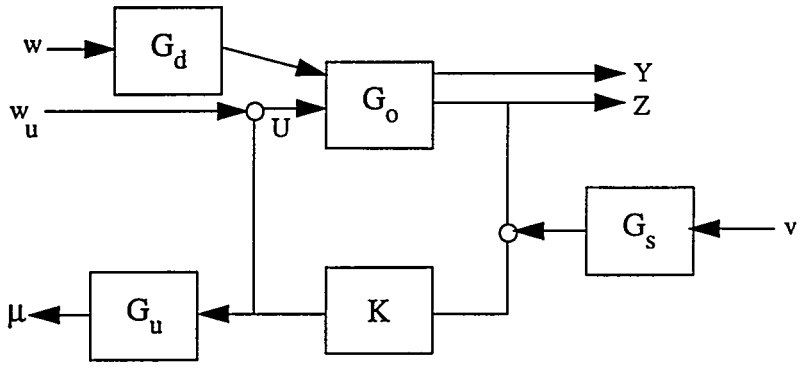

Figure 7. Frequency Weighted System Schematic

The augmented system equations are shown below. The outputs in equation 10, Y and μ are the performances to be minimized and frequency weighted control signal respectively, which are in the *cost function* for FWLQG, equation 13. The signals w, w_u, and v are white zero-mean gaussian stochastic process with

$E\{ww^T\} = W \geq 0 \qquad E\{w_u w_u^T\} = U \geq 0 \qquad E\{vv^T\} = V > 0\ .$

$$\begin{bmatrix} \dot{x} \\ \dot{x}_d \\ \dot{x}_s \\ \dot{x}_\mu \end{bmatrix} = \begin{bmatrix} A & B_w C_d & 0 & 0 \\ 0 & A_d & 0 & 0 \\ 0 & 0 & A_s & 0 \\ 0 & 0 & 0 & A_\mu \end{bmatrix} \begin{bmatrix} x \\ x_d \\ x_s \\ x_\mu \end{bmatrix} + \begin{bmatrix} B_u \\ 0 \\ 0 \\ B_\mu \end{bmatrix} u + \begin{bmatrix} B_w D_d & B_u & 0 \\ B_d & 0 & 0 \\ 0 & 0 & B_s \\ 0 & 0 & 0 \end{bmatrix} \begin{bmatrix} w \\ w_u \\ v \end{bmatrix} \tag{9}$$

$$\begin{bmatrix} Y \\ \mu \end{bmatrix} = \begin{bmatrix} C & 0 & 0 & 0 \\ 0 & 0 & 0 & C_\mu \end{bmatrix} \begin{bmatrix} x \\ x_d \\ x_s \\ x_\mu \end{bmatrix} + \begin{bmatrix} D_u \\ D_\mu \end{bmatrix} u + \begin{bmatrix} D_w & 0 & 0 \\ 0 & 0 & 0 \end{bmatrix} \begin{bmatrix} w \\ w_u \\ v \end{bmatrix} \tag{10}$$

$$Z = \begin{bmatrix} M & 0 & C_s & 0 \end{bmatrix} \begin{bmatrix} x \\ x_d \\ x_s \\ x_\mu \end{bmatrix} + \begin{bmatrix} N_u \end{bmatrix} u + \begin{bmatrix} N_w & N_u & D_s \end{bmatrix} \begin{bmatrix} w \\ w_u \\ v \end{bmatrix} \tag{11}$$

For this design method the cost function to be minimized is shown in equation 12. The two terms that are included in the cost function are y (the performance to be minimized) and μ (the frequency weighted control signal). Where $Q = Q^T \geq 0$ and $R = R^T > 0$ are weighting matrices.

$$J = \lim_{T \to \infty} E\{\int_0^T \left(y^T Q y + \mu^T R \mu \right) dt\} \tag{12}$$

The augmented system matrices and the following weighting matrices can be used with the basic LQG solution shown previously.

$$R_1 = \begin{bmatrix} C^T Q C & 0 & 0 & 0 \\ 0 & 0 & 0 & 0 \\ 0 & 0 & 0 & 0 \\ 0 & 0 & 0 & C_\mu^T R C_\mu \end{bmatrix} \qquad R_2 = D_\mu^T R D_\mu \qquad R_{12} = \begin{bmatrix} C^T Q D_u \\ 0 \\ 0 \\ C_\mu^T R D_\mu \end{bmatrix} \tag{13}$$

$$V_1 = \begin{bmatrix} W & 0 & 0 \\ 0 & U & 0 \\ 0 & 0 & V \end{bmatrix} \qquad v_2 = [V] \qquad V_{12} = \begin{bmatrix} 0 \\ 0 \\ V \end{bmatrix} \tag{14}$$

Maximum Entropy:

Maximum entropy permits the design of robust controllers with respect to structured parametric uncertainty to be determined by the quadratic cost functional. Given a nominal linear system modeled in state space form, equation 1, the parametric uncertainty can be modeled with a set of parameter uncertainty matrices (e.g. $\Delta A, \Delta C, \Delta M, \ldots$ etc.). For example, assuming the parametric error is associated with modal frequency or damping, the only parametric error matrices necessary are for A (i.e. ΔA); however, if these errors are independent or arise from different sources, parametric error matrices can be defined for each source of uncertainty, ΔA_i. The uncertain dynamics of the system can be expressed as shown in equation 15, where $\alpha_i(t)$ is a zero-mean multiplicative white noise process with n uncorrelated error sources.

$$A = A + \sum_{i=1}^{n} \alpha_i(t)\ \Delta A_i \tag{15}$$

With the addition of the multiplicative white noise, the first order state space form of the system dynamics, equation 22, become as shown in equation 16.

$$\dot{x} = \left(A + \sum_{i=1}^{n} \alpha_i(t)\ \Delta A_i \right) x + B_u u + B_w w \tag{16}$$

Once the system dynamics are represented with stochastic differential equations, as shown in equations 17 and 18 the necessary conditions for optimality can be derived [7]. The resulting necessary conditions take the form of two Riccati equations and two Lyapunov equations, coupled by the stochastic parameters. The separation principle which is a foundation of LQG design is invalid in the presence of the parametric uncertainty expressed by maximum entropy. The coupled set of two Riccati and two Lyapunov equations can be solved using homotopy methods. A Pro-Matlab toolbox [8] has been developed to implement the homotopy solution methods for Maximum Entropy robust control design of LQG controllers.

$$dx = \left(A_S\, dt + \sum_{i=1}^{n} d\alpha_i(t) \right) x + B_u u + B_w w \tag{17}$$

$$A_S = A + \frac{1}{2} \sum_{i=1}^{n} \Delta A_i \tag{18}$$

Experimental Evaluation of Frequency Weighted LQG - Maximum Entropy Controllers

Control Design Modelling and Analysis

The model of the Sandia Truss used for control design was a 32 state truncated version of the 54 state ERADC model described in section in which the very uncertain high frequency dynamics above 150 Hz have been truncated. Figure 8 shows a comparison of the actuator - sensor channels for the two models. The low frequency dynamics of the suspension were retained in the control design model even though they are very uncertain and are in a region of low SNR.

The structured singular value, μ, was used in the control design process to analytically evaluate the robust stability of different control designs. Reference 1 provides a brief overview of the structured singular value, μ, and its properties. In the definition of μ, there is an underlying structure, Δ, which for robust stability analysis depends on the uncertainty model of the system. The uncertainty model of the system, Δ, is in a feedback loop with the system dynamics, G_0, and may have structure which correspond to different forms of uncertainty (i.e. additive uncertainty due to unmodelled dynamics or multiplicative uncertainty in the modeshapes at the sensor or actuators, etc.). Robust stability is achieved if stability is guaranteed for all allowable Δ's. Alternatively, the H_∞ norm could be used via the small gain theorem as a measure of robust stability; however, if Δ has structure this approach can be quite conservative. The structured singular value, μ, takes the structure of the perturbation into account and provides a less conservative measure of robust stability. The structured singular value which is a matrix function is defined for a complex matrix, $M \varepsilon \mathbf{C}^{nxn}$ by equation 19. The stability boundary is at $\mu=1$.

$$\mu(M) \equiv \frac{1}{\min \{\bar{\sigma}(\Delta) : (\det(I - M\Delta)=0)\}} \qquad \textbf{(19)}$$

The uncertainty model, Δ, used in the robust stability analysis of the Sandia Truss consisted of three blocks: additive uncertainty, input, and output multiplicative uncertainty. The additive uncertainty weight, Wadd, which is shown in Figure 8, envelops the unmodelled dynamics of the system. The input and output multiplicative uncertainty, W_{io}, was modeled as a frequency dependent weight with 50% uncertainty for frequencies < 3 Hz and 5% uncertainty for high frequency as shown in figure 8. Therefore, the uncertainty model, Δ, used in the robust stability analysis has structure; and, Δ consists of 3 blocks (i.e. additive uncertainty, input multiplicative, output multiplicative).

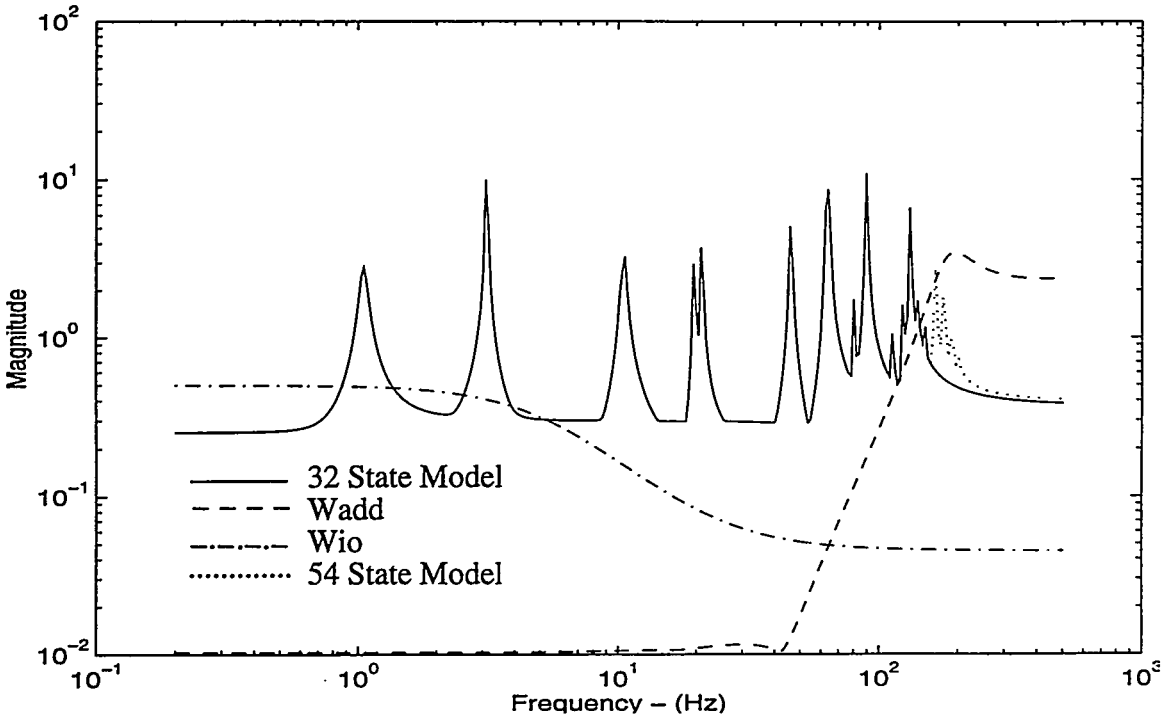

Figure 8. Maximum Singular Value of the actuator - sensor channels of the 54 state and the 32 state control design model.

Frequency Weighted LQG (FWLQG) Controllers

A series of FWLQG controllers of increasing control authority were designed for the initial phase of the study. The purpose of this series of designs were to find the limits of system stability and performance. The control signal weight, G_u, was a diagonal 4-input/4-output, 48 state frequency dependent matrix which is appended to the control design model. The diagonal entries in the control signal weight, G_u, was a band-stop butterworth filter shown in figure 9. The high frequency break point of G_u was chosen to gain stabilize the high frequency unmodelled dynamics of the system(> 150 Hz). G_u was shaped to reduce the system loop gain rapidly in the frequency range 120-150 Hz while the system dynamics are still discrete and reasonably well modelled. The low frequency break point was chosen to stabilize the poorly characterized suspension modes and prevent the propagation of noise in the control loop due to the poor SNR in the low frequency range (<10 Hz). Previous control design studies on this system indicated that coloring of disturbance, G_d, and sensor, G_s, noises was difficult to use in addressing uncertainty without significant loss of system performance. Therefore, the disturbance, w, and actuator, w_d, noises were white with covariances of 3 and 0.5. The sensor noise, v, was chosen to have a covariance 0.01 of the sensor covariance due to w and w_u.

Table 1 summarizes the four frequency weighted LQG designs (Nom1,Nom2, Nom24, Nom27) with increasing control authority which are denoted in table 1 by multiplication of the state weighting matrix, Q, by a scalar of increasing magnitude (e.g. Q*2). The robust

stability μ for these designs are shown in the table. Reduced order 32 state controllers suitable for implementation were obtained by a balanced truncation of the 80 state full order controller. The response of the 120 Hz mode was most affected by controller reduction.

The design Nom1 yielded a stable compensator, K, which also produced a stable closed loop system on experimental implementation. As control authority was increased, the closed loop system was unstable experimentally. The highest authority controller, Nom27, also had an unstable compensator, K.

Figure 10 shows that robust stability degrades (i.e. μ increases) as control authority is increased for the FWLQG designs. μ for the Nom1 controller is well below 1 at all frequencies; however, μ for the Nom27 controller is > 1 for two frequencies in the controller bandwidth, which indicates that the boundary of stability has been crossed. Figure 11 shows a maximum singular value plot for several of the controllers, K, discussed. This figure shows that controller reduction of Nom27 reduced the roll-off at low and high frequency with little effect in the control bandwidth. Due to the nature of the frequency weights used in the FWLQG designs, the controllers have a bandpass nature.

Frequency Weighted LQG with Maximum Entropy (FWLQG/ME) Designs

Several formulations of maximum entropy were studied and designed; however, the controller reported here is Nom27me2. This controller used the same control signal frequency dependent weighting and authority as Nom27; however, frequency uncertainty for the in-band modes from 10 to 120 Hz was incorporated in the ME design. The FWLQG/ME controllers were calculated with homotopy algorithms using the FWLQG designs with no uncertainty for the in-band dynamics as the starting point. The ME controller Nom27me2 is stable; and, the closed loop system was stable with better performance than Nom1. Maximum entropy produced a more robust and stable controller than the FWLQG controller without ME

Also, ME had the effect of lowering the in band gain, reduced the roll-off rate at low and high frequency, and produced a stable controller as well as a stable system. Analytically Nom27me2 also has better robust stability properties than Nom27, figure 10. The gain of Nom27me2 is greater than Nom1 and produced significantly better performance. Figure 12 shows the closed loop experimental performance for the Nom1 and Nom27me2 controllers.

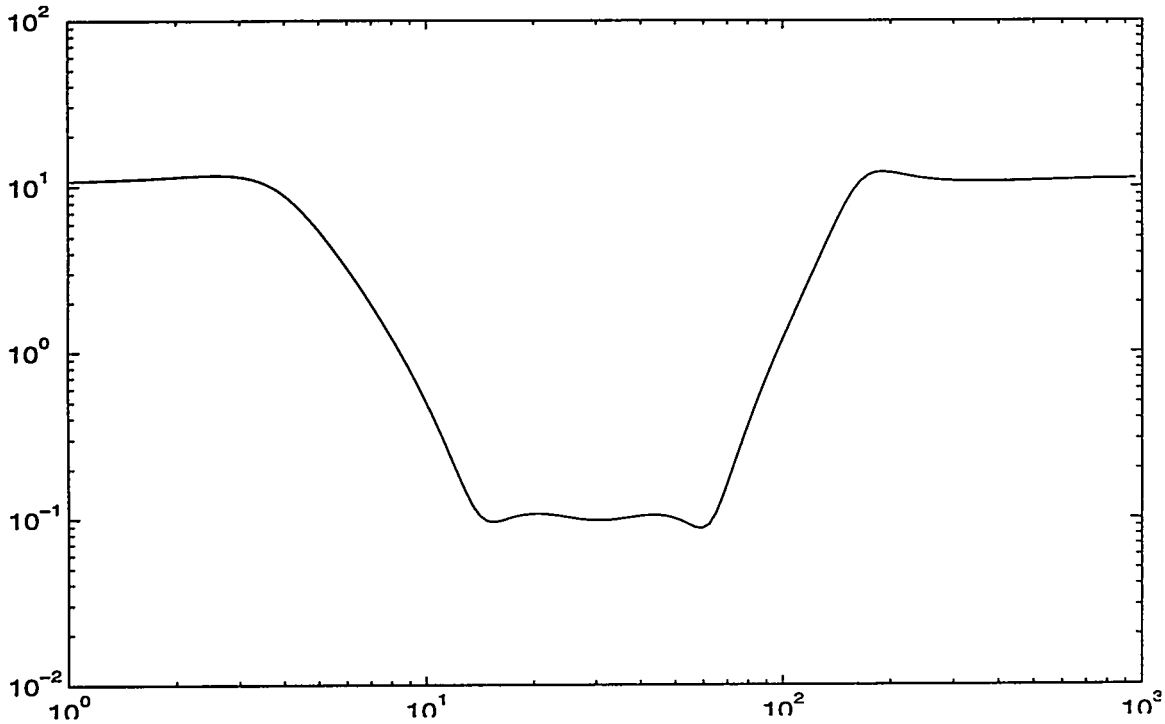

Figure 9. Control Signal Frequency Dependent Weighting, G_u.

Table 1. Frequency Weighted LQG Design Summary

	Design Information			Robust Stability - μ		Comments	
Name	W_u	Q	ME	K_{80}	K_{32}	K stability	System stability[3]
nom1	note 1	Q*1	none	0.47	0.48	stable	stable
nom2	note 1	Q*2	none	0.87	0.92	stable	unstable
nom24	note 1	Q*2.4	none	1.08	1.09	stable	unstable
nom27	note 1	Q*2.7	none	1.13	1.10	unstable	
nom27me2	note 1	Q*2.7	note 2	0.58	0.63	stable	stable

note 1: See Figure 9.
note 2: 2% frequency uncertainty in 10-150 Hz modes.
note 3: experimental assessment of stability

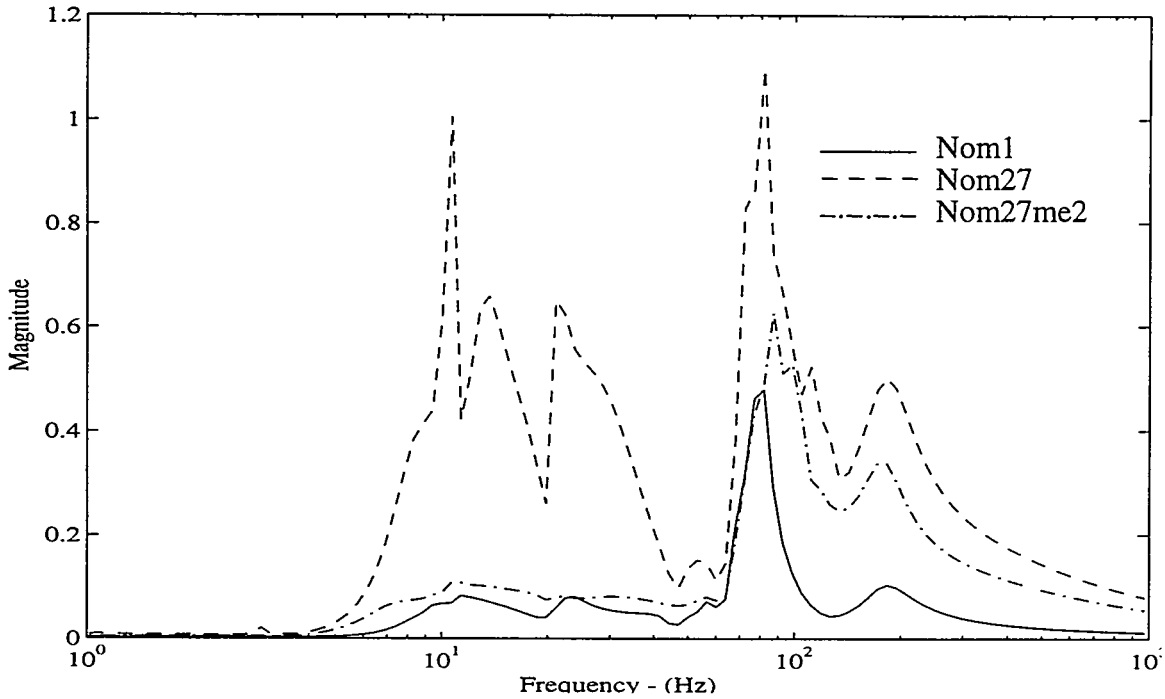

Figure 10. Robust Stability μ (RSMU) for 32 state LQG controllers using Frequency Weighting and Maximum Entropy.

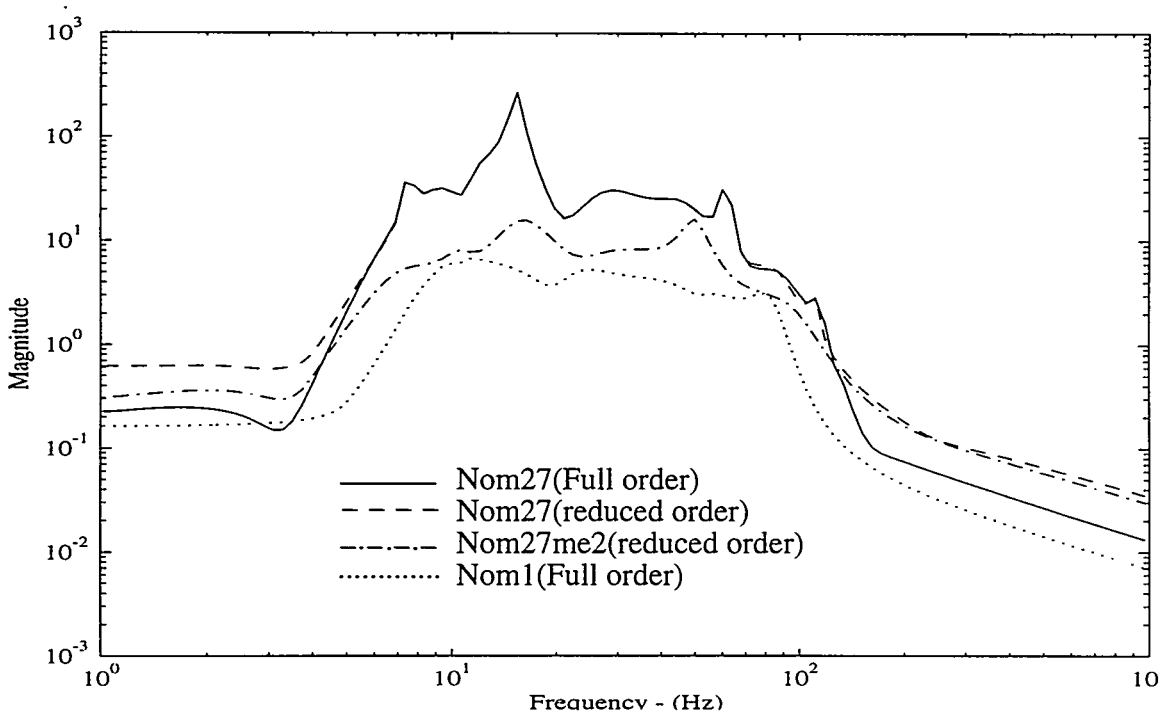

Figure 11. Maximum Singular Value Plots for LQG controllers, K, using Frequency Weighting and Maximum Entropy.

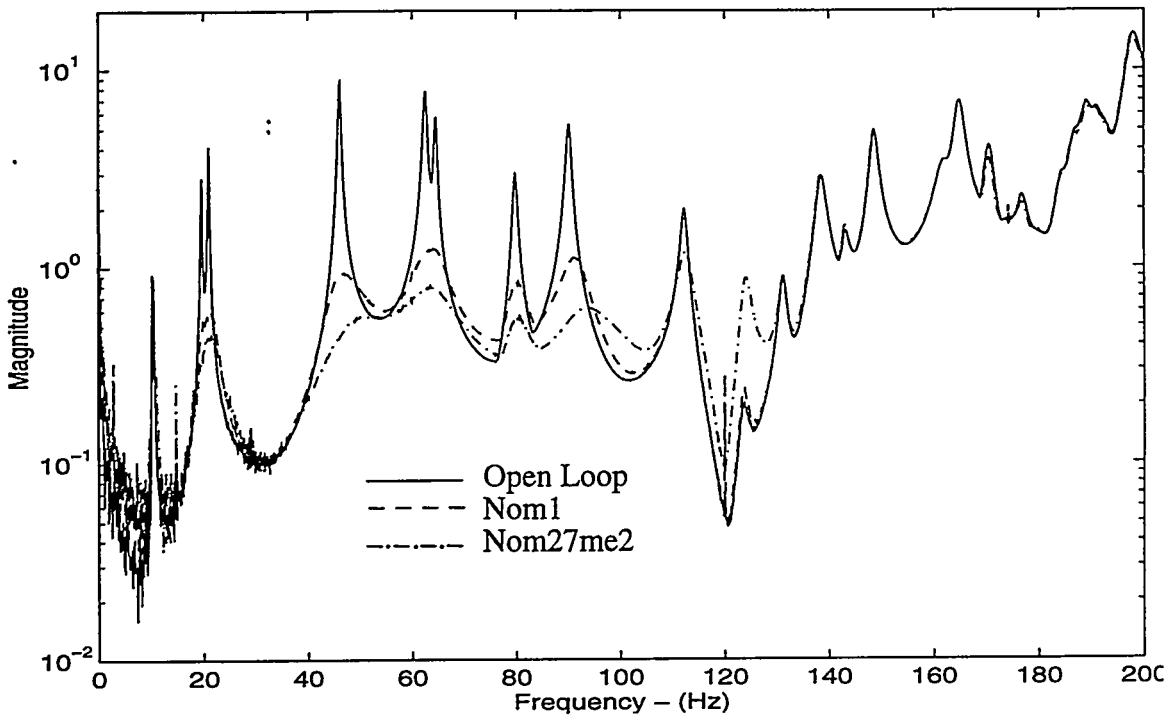

Figure 12. Disturbance-Performance Maximum Singular Value Plots for LQG controllers using Frequency Weighting and Maximum Entropy.

Structured Uncertainty Experiment

In order to experimentally study the effect of maximum entropy on structured uncertainties, the frequency of the 45.9 Hz mode in the *control design model* was perturbed. This produced a mismatch in the system dynamics at 45.9 Hz between the model used to perform control design and the actual system dynamics. Then a FWLQG controller was designed using the same weighting's as the Nom27 controller in which the system was analytically stable. The magnitude of the frequency perturbation was increased until the closed loop system was unstable.

Figure 13 shows the experimental closed loop performance for the FWLQG controller (P30) with the maximum frequency perturbation which still produced an experimentally stable closed loop system. Figure 13 shows that the 45.9 Hz mode is destabilized.

Now a FWLQG/ME controller (P30me) was designed which incorporated frequency uncertainty for the 45.9 Hz mode into the control design. Figure 13 shows the experimental closed loop performance for the FWLQG/ME controller, which stabilized the 45.9 Hz mode and improved system performance.

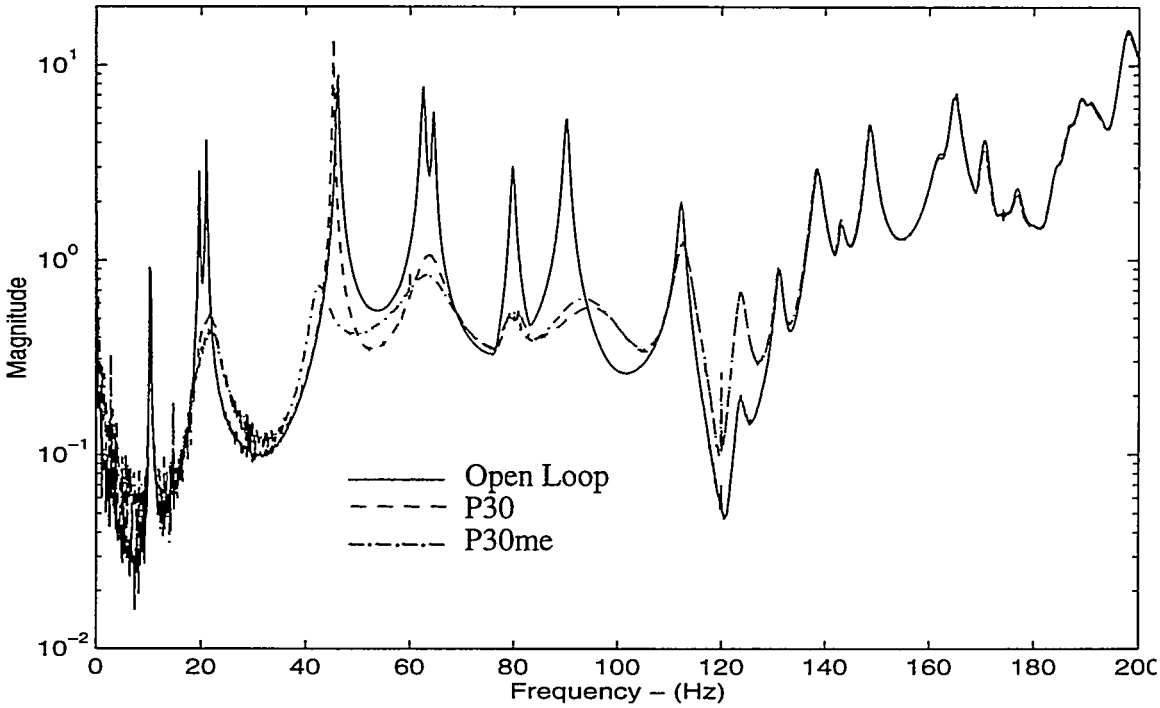

Figure 13. Comparison of FWLQG and FWLQG/ME experimental closed loop performance with a perturbed control design model.

μ-Synthesis Control Design

Background:

μ-synthesis is a control design methodology which has been developed to design controllers which satisfy robust performance and stability requirements [1,15,16]. μ-synthesis integrates, H_∞ controller synthesis and the structured singular value (μ) control analysis into a systematic design methodology.

The basic concepts of μ-synthesis can be explained in the context of a general system interconnection structure of plant dynamics (P), controller (K) and uncertainty (Δ) shown in Figure 14. The objective of the H_∞ control problem is to find a stabilizing controller, K, which minimizes $\min_K \|G_{22}\|_\infty$ for the nominal system (Δ=0). State space methods of obtaining these solutions are discussed in References 1 and 15. The minimization is done using an iterative scheme (γ iteration). The stability bounds of the system due to the uncertainty Δ can be evaluated using the H_∞ norm and the small gain theorem; however, this approach has been shown to be overly conservative when the uncertainty Δ has structure. To handle limitations of the H_∞ norm measure of uncertainty, the structured singular value, μ has been developed. The structured singular value is a matrix function which assumes that the uncertainty Δ has an underlying structure prescribed by a set, $\underline{\Delta}$, of scalar or full block, diagonal matrices. The structure of Δ for a particular problem is related to the uncertainty and performance objectives. The structured singular value, μ, is defined in equation 20. The structured singular value, μ, can be calculated using an algorithm in which a frequency dependent scaling matrix, D, with the same structure as Δ is used to produce a tight bound on the magnitude of μ.

$$\mu(G_{11}(j\omega)) \equiv \frac{1}{\min\{\bar{\sigma}(\Delta(j\omega)) : (\Delta \in \underline{\Delta})\ (\det[I - G_{11}(j\omega)\Delta(j\omega)] = 0)\}} \quad (20)$$

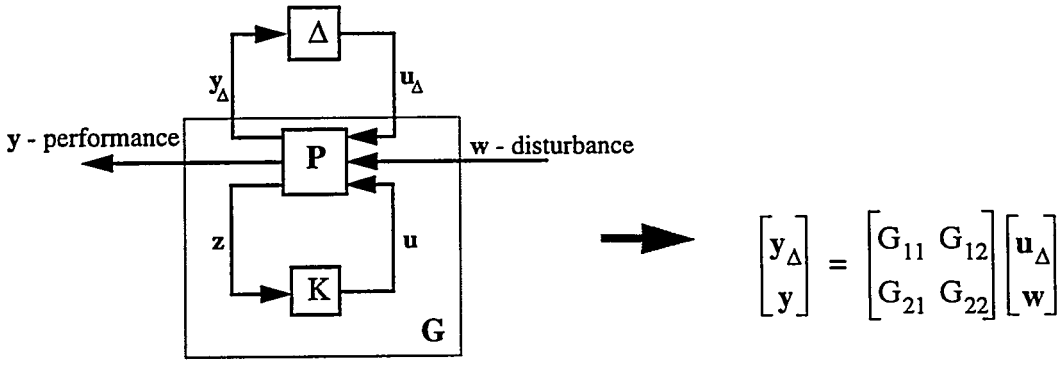

Figure 14. General Interconnection Structure

The problem of μ synthesis robust control design is to find a stabilizing controller K and a scaling matrix D which minimize the function shown in equation 21. D-K iteration is an algorithm capable of accomplishing this task; however, global convergence cannot be guaranteed. During each iteration, the D scalings are realized as stable minimum phase transfer functions and *wrapped* into the system interconnection structure, which cause the order of the design problem and hence the resulting controller to increase with twice the order of the D scales.

$$\min_{D,K} \left\| DG_{11}D^{-1} \right\|_\infty \tag{21}$$

Terminology and Definitions:

The following terms are used in the analysis of controllers discussed in this report.

Uncertainty (Δ): The system uncertainty is structured and normalized such that $\bar{\sigma}(\Delta) \leq 1$.

Nominal System: The system dynamics with Δ=0;

Nominal Stability: The nominal plant model, P, must be stabilized by the controller, K.

Nominal Performance (NP): The nominal closed loop system must satisfy the performance requirements, equation 22.

$$\left\| G_{22} \right\|_\infty < 1 \tag{22}$$

Robust Stability - structured uncertainty (RSMU): If equation 23 is satisfied, stability is guaranteed for all allowable structured Δ's and frequencies ω.

$$\sup_\omega \mu(G_{11}) \leq 1 \tag{23}$$

Robust Performance - structured uncertainty (RPMU): If equation 24 is satisfied, performance is maintained in the presence of all allowable structured Δ's and frequencies ω. The μ test of equation 24 is calculated with respect to $\underline{\Delta} = \{\mathrm{diag}[\Delta\ \Delta_p]\}$, where a performance uncertainty, Δ_p with $\bar{\sigma}(\Delta_p) \leq 1$ can be associated with the performance, equation 22.

$$\sup_\omega \mu(G) \leq 1 \tag{24}$$

Control Objectives

The control design objective for this system can be stated as follows:

- Minimize the elastic response of the system at the performance locations (i.e. x,y,z response of the plate at the top outboard bay) in the frequency range of 10 - 120 Hz, while satisfying the following criteria:
- Maintain system stability and performance in the face of high frequency uncertain or unmodelled dynamics.
- Do not excite the low frequency suspension dynamics of the system (<10 Hz) whose dynamics are poorly characterized.

Control Design

This section will discuss the details of the μ-synthesis control design formulation for the Sandia Truss, and the analytical control design results. Since the processor used to implement the control law was limited to 32 states, the impact of controller reduction will also be discussed.

The basic description for a μ-synthesis control design is the system interconnection structure which expresses the uncertainty, disturbance and performance modelling of the system. The interconnection structure for the Sandia truss is shown in Figure 15. The uncertainty, disturbance and performance requirements are normalized to 1, which is accomplished by the weighting matrices W_u, W_{in}, W_{out}, W_{add}, W_{perf}. The details of the models for the Sandia truss dynamics, uncertainty and performances descriptions are discussed below.

Sandia Truss Dynamics(P): The control design model of the *Sandia Truss*, Figure 2, was a 32 state model which was a truncated version of the 54 state ERADC model in which the very uncertain high frequency dynamics above 150 Hz have been truncated. Since the performance is desired in the frequency range of 10-120 Hz., the control design model still retains some well characterized dynamics in the controller roll-off region of 120-150 Hz. Figure 16 shows the actuator - sensor transfer function maximum singular value for the Sandia truss 32 state and 54 state models.

Additive Uncertainty(Wadd): Since the Sandia truss dynamics model (P) used in the control design only represented the system dynamics from 10 Hz - 150 Hz, there is additive uncertainty in the control design model due to the unmodelled dynamics. The additive uncertainty weight matrix, Wadd, which is in parallel to the Sandia truss dynamics, P, must envelop the possible magnitude of unmodelled system dynamics encountered. Wadd is a 24 state, 4x4 diagonal frequency dependent weighting matrix, that is composed of 4 weights which envelope the maximum singular value of the unmodelled dynamics of each actuator to all control sensors. The additive uncertainty weights had a low value at frequencies below 150 Hz and envelopes the full order actuator to sensor transfer function maximum singular value above 150 Hz since these dynamics were truncated. These 4 frequency dependent weights were then multiplied by a single scalar until they enveloped the maximum singular value of the unmodelled dynamics for all actuators to all sensors as shown in Figure 16. This method of choosing Wadd allowed each actuator to be individually constrained by the additive uncertainty.

Input/Output Multiplicative Uncertainty(Win/Wout): Multiplicative Uncertainty on the actuators(actuators) or sensors(output) model the uncertainty of the system eigenvectors at the system input or output. The weightings for input and output multiplicative uncertainty (Win and Wout respectively) were modeled as diagonal scalar matrices with an initial value of 0.001, which minimized appended states to the interconnection model and essentially removed input and output multiplicative uncertainty as an active design constraint from the problem for the initial set of designs.

Performance (Wperf): The disturbance response in the three coordinate directions at the top of the Sandia truss are to be minimized in the range of 10-120Hz which includes the first 10 elastic modes of the system. The performance outputs were formed in the interconnection structure by zeroing the modal participation factors (i.e. entries in the B and C matrices of the state space model) for the other system dynamics. The performance weight, W_p was taken as an identity matrix multiplied by a constant which specified the desired level of performance. This approach was taken to achieve a performance metric which conflicted as little as possible with the additive uncertainty and the desire to not excite the suspension dynamics < 3 Hz.

Control Signal(Wu): The control effort was penalized by a diagonal weighting matrix, Wu. The purpose of Wu was to limit the control effort in the low frequency region (<10Hz) where unmodelled dynamics and a low SNR exists. Several different frequency dependent weights, Wu, were used to study the effects on the closed loop system. Figure 17 shows the frequency dependence of the Wu weighting matrices used in this study. Wu0 is a diagonal scalar weighting matrix which was chosen to be 0.1 (i.e. desired control signal <10 volts over all frequencies). Wu1 (first order, 4 state) and Wu2 (second order, 8 state) diagonal frequency dependent weighting matrices which were penalizing low frequency control signal to various degrees. For example both Wu1 and Wu2 require that the low frequency control signal be <0.01 volts and the high frequency control signal <10 volts; however, the transition of the constraints are different.

Uncertainty Blocks (Δp, Δi,Δo,Δa): The structure of the uncertainty blocks were defined as follows: Δ_p - full 3x7 block, Δ_i - full 4x4 block, Δ_a - full 7x4 block, Δ_o - full 7x7 block.

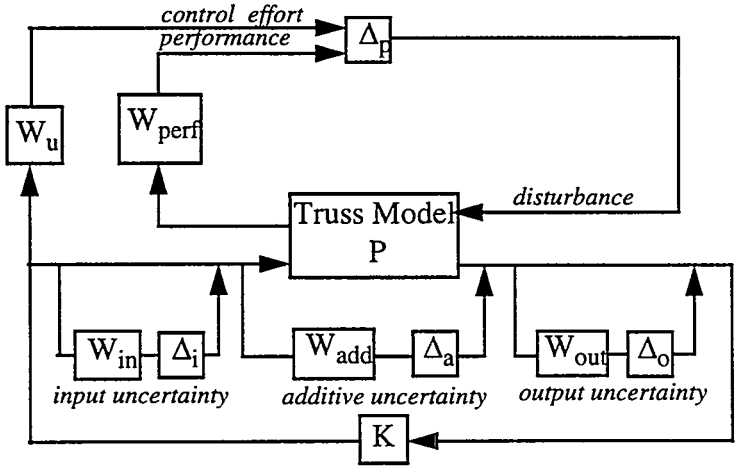

Figure 15. Sandia Truss Interconnection Structure.

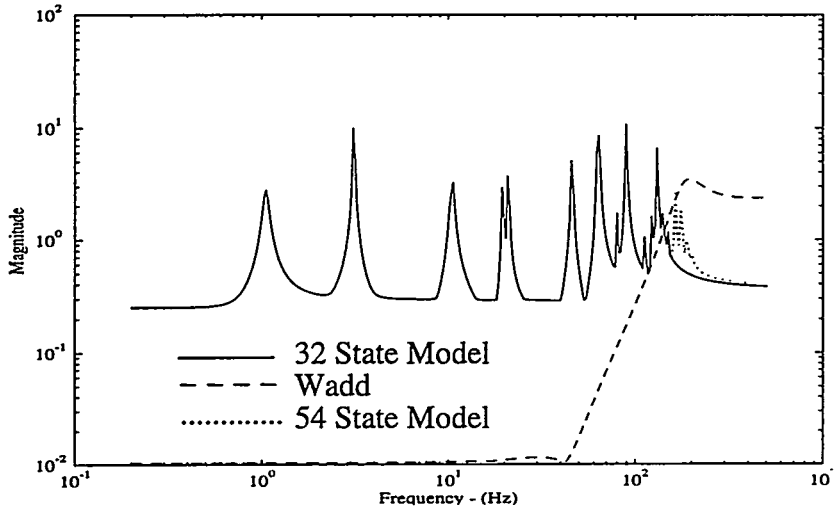

Figure 16. Full and Reduced Order Control Design Model Actuator to Sensor Transfer Function and Additive Uncertainty Weight Maximum Singular Value Plots.

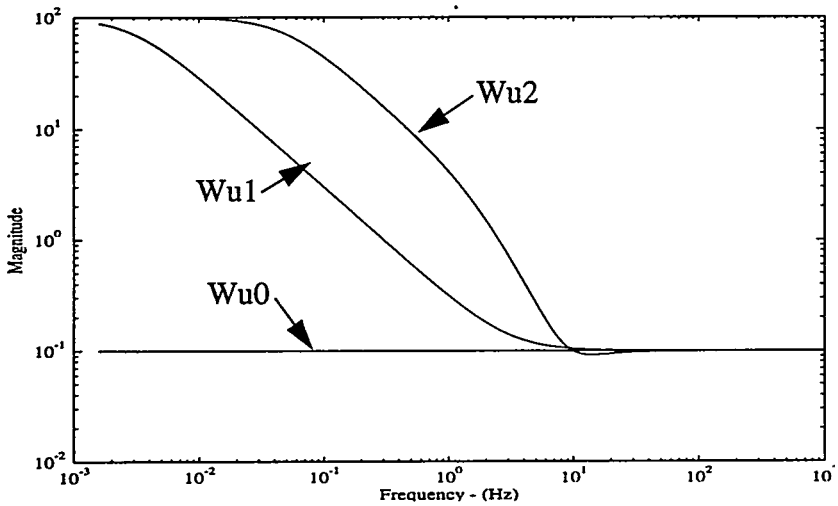

Figure 17. Control Signal Weights, Wu.

Experimental Evaluation of μ-Synthesis Controllers

μ-Synthesis Controllers with Control Signal Weighting

A number of controllers were designed using different weightings for the control signal, performance, and additive uncertainty. The μ-Analysis and Synthesis Toolbox [16] was used to calculate the μ-synthesis controllers. Table 2 presents design, performance and robustness information on the full and reduced order (32 state) controllers. The 32 state reduced order controllers were obtained via a balanced truncation. There were three series (S,T,U) of controllers designed in which control signal weights, Figure 17, were the major difference.

The S series of controllers used the control signal weights(Wu0), which was to limit the control signal < 10 volts. The controller resulting from this design tended to have significant control signal at low frequencies as shown in Figure 18. On implementation this resulted in a low frequency excitation of the Sandia truss suspension and occasional sensor channel saturations.

The T series of controllers used the frequency dependent weight Wu1 for the control signal and the additive uncertainty weight was multiplied by 1.7. The additive uncertainty was increased due to the inability to determine if the channel saturation was a low or high frequency phenomena. The T series of controllers reduced the low frequency excitation of the truss suspension.

The U series of controllers used the control signal weight Wu2, which had a sharper transition region, Figure 17. The U series of controller did not excite the suspension dynamics when implemented. The initial U series controllers (U1.5,U2) maintained the increased additive uncertainty weight (1.7*Wadd); however, this constraint was eased (1.0*Wadd) in subsequent designs(U2.5), when it became obvious from implementation that spillover as a result of additive uncertainty was not occurring. Figure 18 show the effect of different control signal weightings (Wu0,Wu1,Wu2) on the maximum singular value of the disturbance-control signal closed loop transfer function.

The full order μ-synthesis controllers are quite large (>100 states), due to the need to append frequency dependent weightings to the interconnection structure to express control design constraints, and D-K iterations which require the fitting and incorporation of frequency dependent D-scales into the interconnection structure. Figure 19 shows that controller reduction effected the high and low frequency roll-off of the U2.5 controller. The other controllers discussed in this study showed similar effects. Table 2 shows that performance and robustness properties are degraded during controller reduction. An analytical study showed that if a 60 state controller was able to be implemented the performance and robustness degradation would be minimal. Figure 20 show the performance and robustness properties of controller U2.5 as a function of frequency. Nominal performance (NP) is met for the full order controller except for the mode at 120 Hz, which is probably due to inefficient actuator placement for this mode. NP is degraded

for the suspension dynamics due to controller reduction which reduced the controller roll off in this region. The structured robust stability μ test (RSMU) is satisfied for both full and reduced order controllers, and was not significantly affected by controller reduction. The structured robust performance μ test (RPMU) was affected by controller reduction in a similar manner to NP.

Figure 22 shows the maximum singular value of the disturbance to performance transfer function for the experimental control implementation. Spillover or noise propagation was not observed in the U series of controllers, however, a slight enhancement of a mode at 150 Hz was observed. Figure 21 shows that the loop gain at 150 Hz is <1. The controller has a sharp roll-off between 120 and 150 Hz, Figures 18 and 19, in order to meet performance and additive uncertainty requirements; however, the inclusion of the well characterized dynamics of that region in the control design model maintained system stability.

Table 2. Controller Design, Robustness and Performance Information

	Design Information			Full Order Controller				32 state Controller			
Name	Wperf	Wu	Wadd	#states	NP	RSMU	RPMU	NP	RSMU	RPMU	comments
S1	1.0	Wu0	1.0*Wadd	118	0.766	0.082	0.776	0.789	0.088	1.078	suspension excitation
T1	1.0	Wu1	1.7*Wadd	133	0.783	0.143	0.791	0.846	0.162	0.853	suspension excitation
U1.5	1.5	Wu2	1.7*Wadd	151	0.866	0.199	0.916	1.42	0.2	1.424	Stable
U2	2.0	Wu2	1.7*Wadd	151	1.018	0.245	1.115	1.73	0.245	1.73	Stable
U2.5	2.5	Wu2	1.0*Wadd	148	1.35	0.172	1.424	1.87	0.172	1.88	Stable

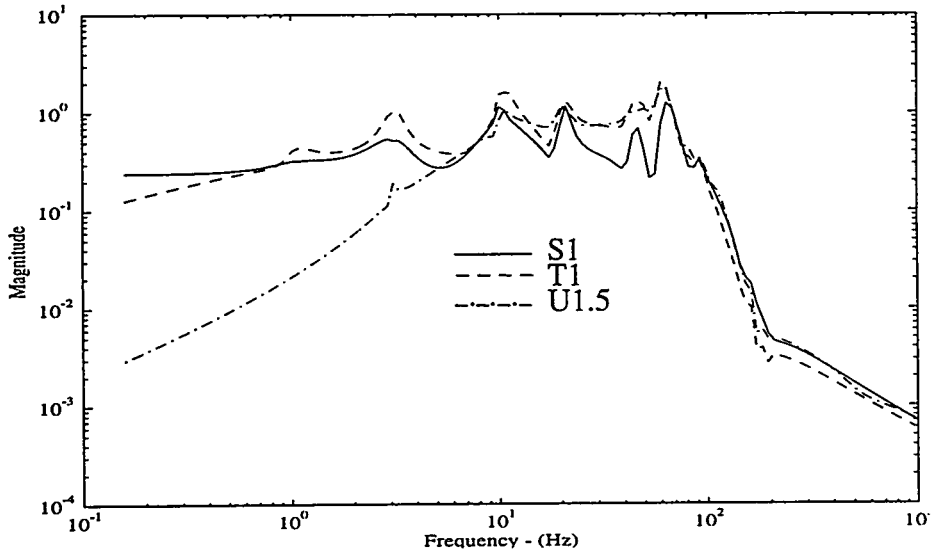

Figure 18. Disturbance to Control Signal Maximum Singular Value versus Frequency for the Full Order Controllers S1,T1,U1.5 .

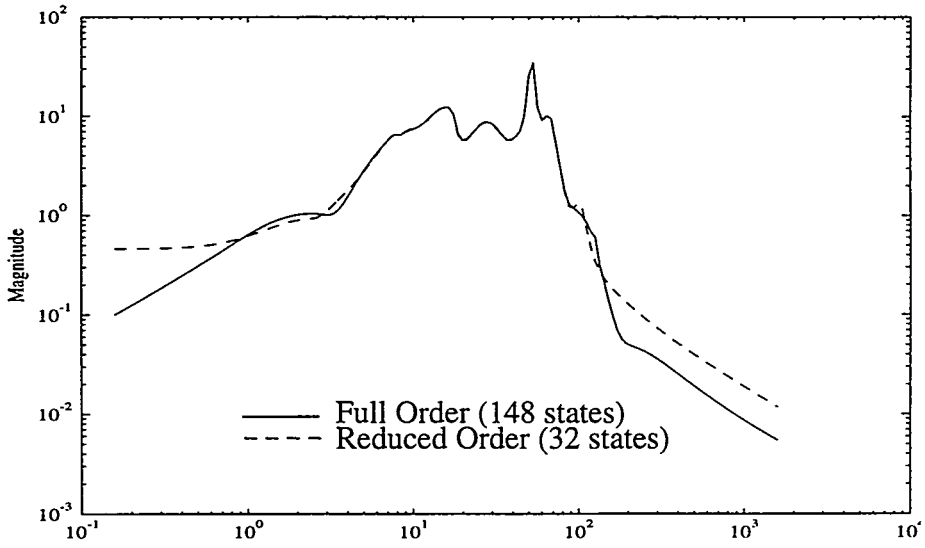

Figure 19. Maximum Singular Value versus Frequency for Controller U2.5

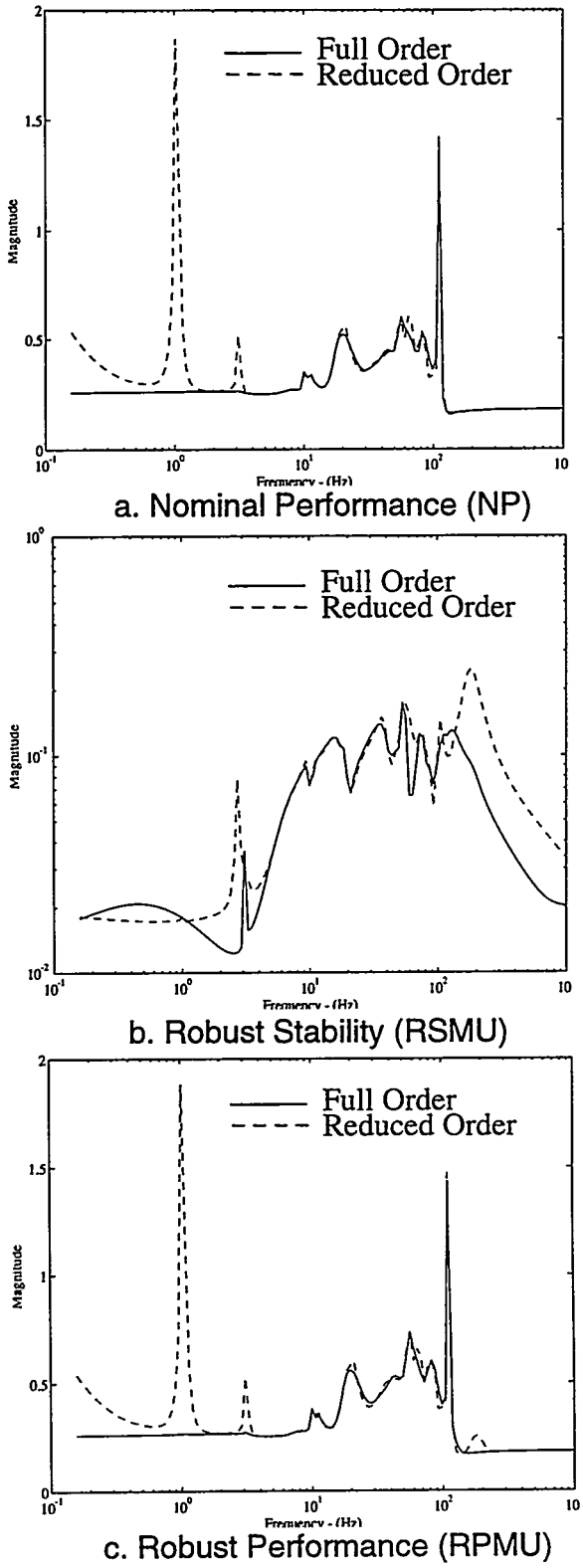

Figure 20. Nominal Performance, Robust Stability and Robust Performance for Full and Reduced Order Controller U2.5

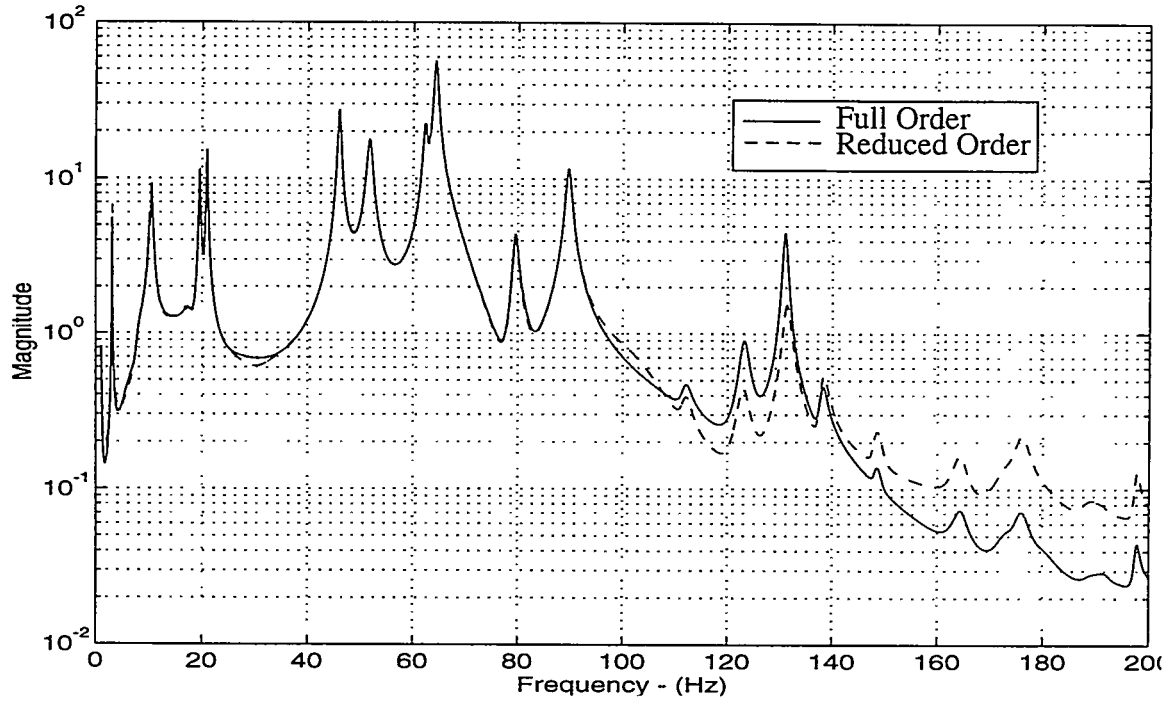

Figure 21. Loop Gain Maximum Singular Value Plot.

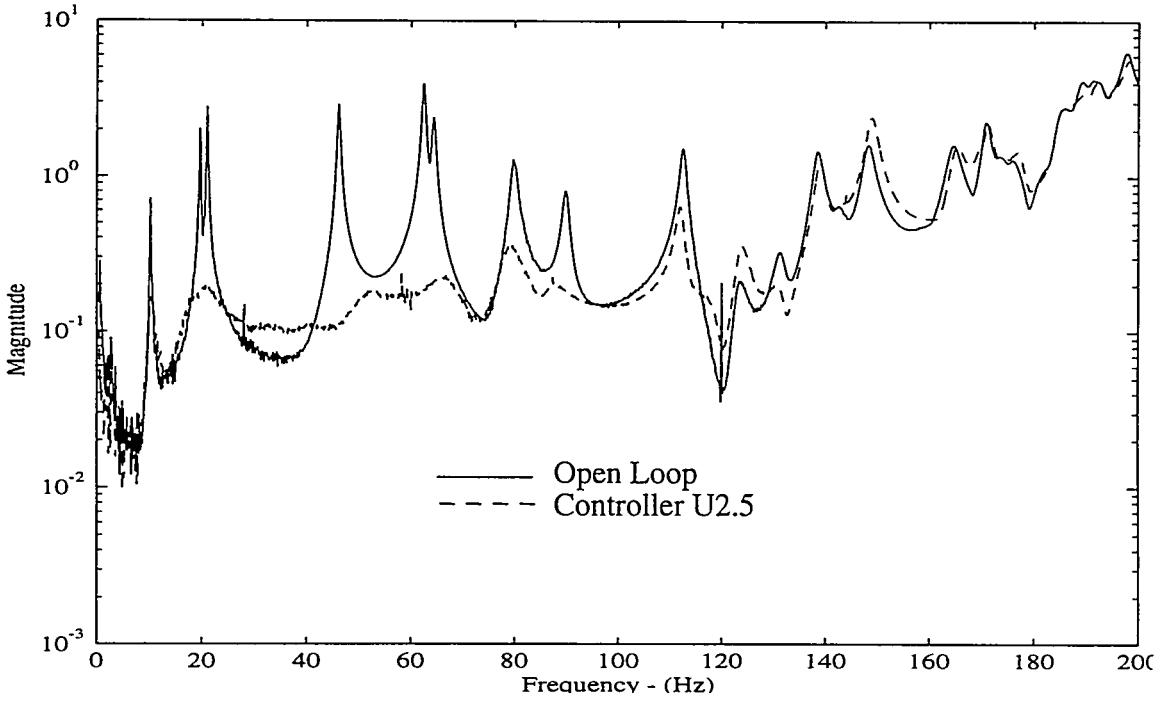

Figure 22. Maximum Singular Value of the Experimental Disturbance - Performance Transfer Function

Alternative Uncertainty Models

One of the principal control design difficulties for this system was to prevent the excitation of the system suspension dynamics and prohibit the propagation of noise in the low frequency region. The control design model was also inaccurate in this region due to a low signal to noise and unmeasured input from the environment. The method described in the previous section for dealing with this control design problem was to constrain the control signal magnitude in this frequency range to a small value by appending a frequency dependent weight to the control interconnection structure used for design. This section will briefly describe three alternate approaches to this control design problem.

1. Model the low frequency uncertainty in the control design model as multiplicative uncertainty at the system input. (MSIO)

2. Model the low frequency uncertainty as a parametric uncertainty of the modal stiffness parameters for the suspension dynamics of the control design model. (dK)

3. Model the low frequency uncertainty as a parametric uncertainty of the input/output matrices (B,C) for the suspension dynamics in the state space control design model. (dBC)

The dK and dBC approaches use a parametric uncertainty model to express the uncertainty at low frequency. The methodology for modeling parametric uncertainty used in this study is discussed in detail by reference 17. The comparison the results of the parametric uncertainty methods (dK and dBC) with the approaches using input multiplicative uncertainty or control signal weighting, will illustrate the characteristics and applicability of these approaches to a physical system.

A series of controllers with varying amounts of uncertainty were designed with the three alternative uncertainty models. Table 3 lists the full and reduced order design, performance and robustness information for a representative controller of each type. The μ-synthesis design of the two parametric uncertainty designs DK2 (20% suspension modal stiffness uncertainty) and DBC2 (20% suspension mode input/output matrix uncertainty) were performed with complex μ. Figure 23 shows the frequency dependent weight, Win, used to specify the input multiplicative uncertainty used in the design, MSIO. Win was a diagonal 4x4 frequency dependent weighting matrix. Input multiplicative uncertainty was used in this design because it would involve fewer frequency dependent weights (4 actuators versus 7 sensors), hence keeping the design problem somewhat smaller. Win specifies 50% uncertainty at low frequency and small uncertainty at high frequency.

The DK2 and DBC2 controllers were unstable upon implementation. This was due to the high DC gain of the controllers in the noisy low frequency environment, which was the dominant physical phenomena. It should be noted that the DK series of controllers tended to *notch filter* the uncertain dynamics at high level of uncertainty (%50). The DBC controllers somewhat reduced the low frequency gain of the system as can be seen in Figure 24.

The input multiplicative uncertainty controller MSIO proved to be a viable alternative formulation for this control design problem. MSIO controller gain is reduced in the region of high input multiplicative uncertainty, Figure 24. Figure 25 shows the experimental open and closed loop maximum singular value of the disturbance to performance transfer functions.

Table 3. Controller Design, Robustness and Performance Information for Alternative Uncertainty Formulations

	Design Information					Full Order Controller				32 state Controller		
Name	W_p	W_u	W_{add}*#	W_{in}&W_{out}	P_Δ	order	NP	RSMU	RPMU	NP	RSMU	RPMU
dK2	2.0	0.1	1.0*Wadd	0.001/0.001	K*0.2	176	0.90	0.57	0.77	1.20	0.57	1.25
dBC2	2.0	0.1	1.0*Wadd	0.001/0.001	BC*0.2	188	0.95	0.36	1.18	1.13	0.36	1.22
MSIO	2.0	0.1	1.0*Wadd	Win/0.001	N/A	239	0.63	0.20	0.76	1.13	0.20	1.16

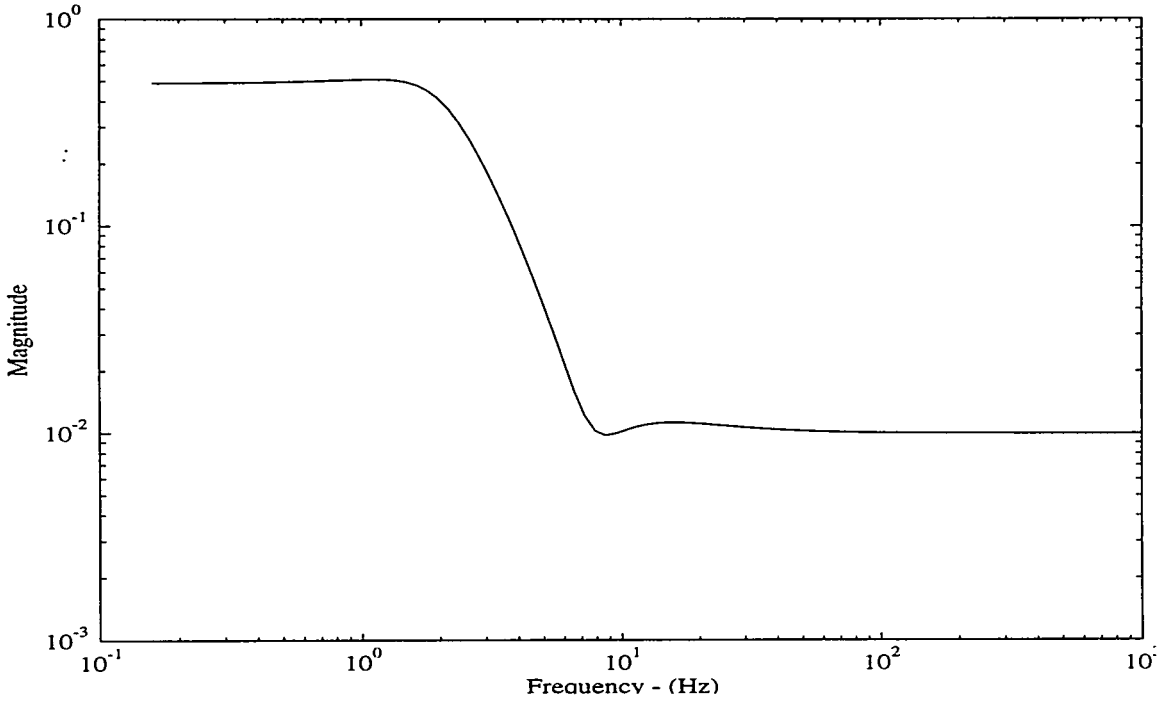

Figure 23. Input Multiplicative Weight - Win.

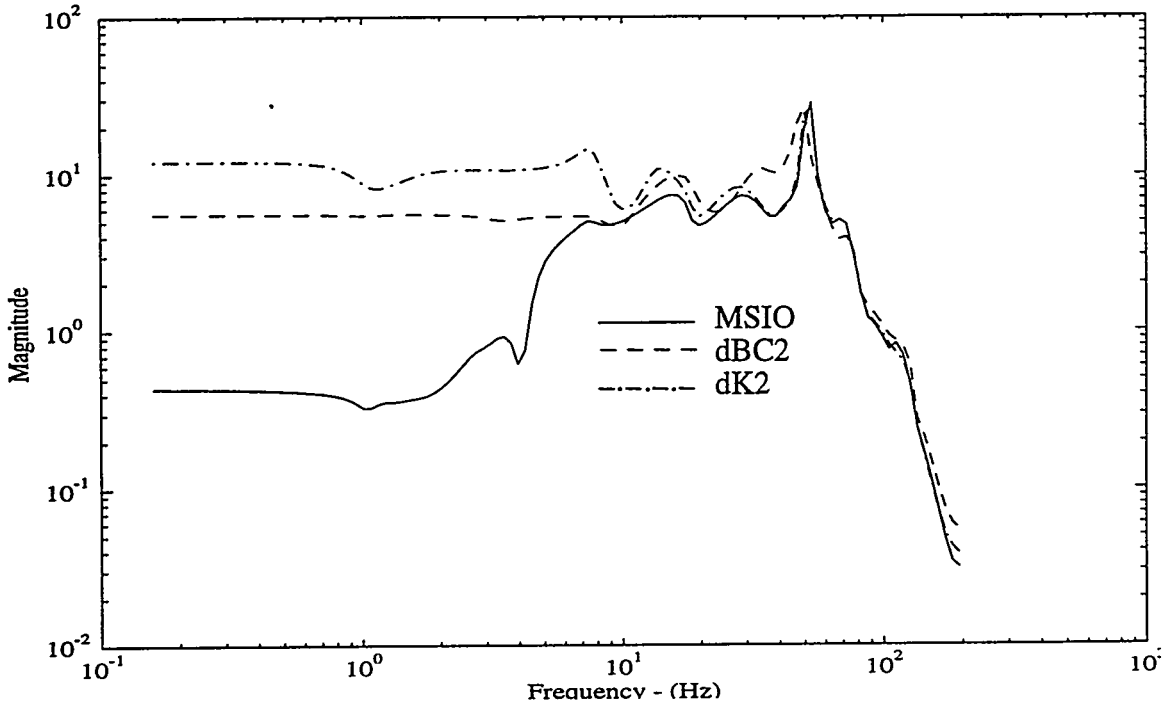

Figure 24. Controller Maximum Singular Value Plot.

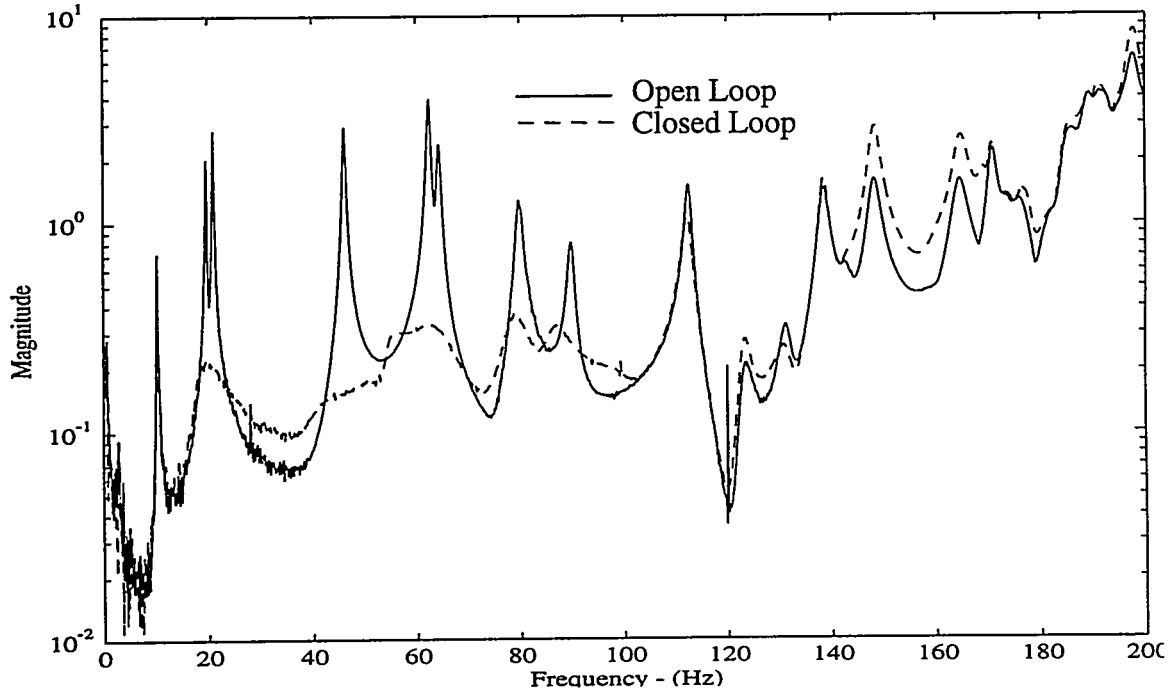

Figure 25. Maximum Singular Value of the Experimental Disturbance - Performance Transfer Functions.

Summary and Conclusions

This project evaluated the abilities of system identification using the eigensystem realization algorithm with data correlation (ERADC) and two MIMO control design methodologies. The control design method that were implemented are frequency weighted LQG (FWLQG) with maximum entropy (ME), and μ-synthesis. Several SISO active damping methods (e.g. velocity feedback, positive position feedback etc.) were investigated in this project but will be reported separately. The Sandia Truss was used as the experimental testbed for identification and control design studies.

A full order (54 state) control design model was identified using ERADC. The control design model was quite accurate in the frequency range of 10 - 150 Hz. However, above 150 Hz the system dynamics became quite dense due to localized dynamics of the truss. Below 10 Hz the dynamics were poorly identified due to significant unmeasured disturbances during the measurement of the system frequency response functions. Experimental system identification using the ERADC algorithm minimized the time to obtain an control design model. The complex mode indicator function was used to estimate the system order, system roots and provide a figure of merit for the control design model. Multiple data sets were required to improve the SNR over the low frequency range.

FWLQG was shown to be capable of control design with a specified bandwidth and gain stabilization of additive uncertainty due to unmodeled dynamics. However, FWLQG was shown to be sensitive to structured uncertainty of in-band system dynamics. Maximum entropy provided increased robustness properties for the controller. Maximum entropy reduced the gain and roll-off rate of the controller as well as producing a strong stabilizing controller. An experimental demonstration of the ability of maximum entropy to stabilize a structured (frequency) uncertainty in the system dynamics was performed. In order to achieve specified constraints, the LQG method with frequency weighting and maximum entropy is not explicit and requires iterative design. Homotopy methods were necessary to calculate the maximum entropy controllers; however the computational burden was not prohibitive.

MIMO (4 actuators/7 sensors) μ-synthesis controllers were designed for the Sandia Truss which produced good performance and robustness properties. μ-synthesis produced high order controllers as a result of the D-K iteration algorithm which were reduced to 32 states for implementation by a balance truncation. The controller reduction process caused some degradation of controller performance and robustness properties. Analytical studies showed that 60 state controllers could be implemented on this system with minimal degradation of controller properties. Two approaches of modeling the system uncertainty at low frequency (control signal constraint, input multiplicative uncertainty) were successful in the implementation of μ-synthesis controllers. The use of parametric uncertainty to model the uncertain suspension dynamics was not experimentally successful due to the high gain at low-frequency of the dK and dBC controllers. The controllers developed from using parametric uncertainty modeling tended to make localized modifications to the controller associated with the nature of the parametric uncertainty. For example, the parametric modal stiffness uncertainty controller (dK) tended to *notch filter*

the uncertain suspension dynamics for high uncertainty levels. This approach proved to not be physically practical for this application, in which the noise environment in the low frequency region was the dominant physical phenomena. This illustrates the need for physical understanding of the system dynamics in order to select the appropriate method for modeling system uncertainty.

The FWLQG/ME and the μ-synthesis controllers produced approximately the same level of performance, Figures 12, 22 and 25. The FWLQG/ME required iterative designs with various levels of ME and frequency weightings in order to design controllers with high performance and adequate robustness properties. The FWLQG/ME full order controllers consisted of 80 states. The μ-synthesis controllers were designed using D-K iteration as implemented in the μ-Tools Pro-Matlab software, which is a very computer intensive iterative process which requires human intervention/judgement in the fitting of the frequency dependent D-scales. This procedure for the μ-synthesis controllers is not guaranteed to converge and is somewhat sensitive to the fitting of the frequency dependent D-scales. The full order μ-synthesis were quite large (>100 states); but, controller reduction using a balanced truncation was not difficult since a large number of the states were of little significance. From the point of view of a control designer the practical trade-off between these two control design methods *for this application* appeared to be the following two points.

- The order of magnitude greater computational and controller reduction effort for μ-synthesis versus FWLQG/ME.

  versus

- The orderly mathematical expression of the control design problem and constraints with μ-synthesis. FWLQG/ME required iterative designs with various selections of weightings etc.

Of course there are a number of other issues which will provide impetus for the use of one method over another in a particular application such as:

- The impressive abilities of maximum entropy to robustify a control law. It would be very interesting to see an experimental comparison of μ-synthesis using real μ versus maximum entropy.
- The applicability of minimizing the H_∞ norm versus the H_2 norm for disturbance rejection problems such as the application demonstrated in this project. The performance results achieved in this project were very comparable.

ERADC, μ-synthesis and FWLQG/ME are all powerful methods. Physical insights and engineering judgement are required, to obtain a high performance robust control system for structural control applications using any of these methods.

References

[1]Maciejowski, J. M., *Multivariable Feedback Design*, Addison-Wesley, 1989.

[2]Hyland, D. C., Junkins, J. L., Longman, R. W., "Active Control Technology for Large Space Structures," *Journal of Guidance, Control and Dynamics*, Vol. 16, No. 5, Sept. - Oct. 1993.

[3]Doyle, J.C., "Guaranteed Margins for LQG regulators," *IEEE Transactions on Automatic Control*, Vol. AC-23, No. 4, Aug. 1978, pp. 756-757.

[4]Gupta, N. K., "Frequency-Shaped Cost Functionals: Extension of Linear-Quadratic-Gaussian Design Methods", *J. Guidance and Control*, Vol. 3, No. 6, Nov.-Dec. 1980.

[5]Safonov, M. G., "Feedback Properties of Multivariable Systems: The Role and Use of the Return Difference Matrix", *IEEE Trans. Automat. Contr.*, AC-26, no. 1, pp47-65, Feb. 1981.

[6]Opdenacker, Ph. C., et al, "Reduced-Order Compensator Design for a Flexible Structure", *J. Guidance and Control*, Vol. 13, No. 1, Jan.-Feb. 1990.

[7]Bernstein, D. S., and Greeley, S. W., "Robust Controller Synthesis Using the Maximum Entropy Design Equations," IEEE Transactions on Automatic Control, Vol. AC-31, April 1986, pp.362-364.

[8]Collins, E. G., Davis, L. D., Richter, S., "Homotopy Algorithms for H2 optimal Reduced Order dynamic compensation and Maximum Entropy control", Harris Corporation, Government Aerospace Systems Division, GASD-HA0, November 1992.

[9]Collins, E. G., Jr., Phillips, D. J., and Hyland, D. C., "Design and Implementation of Robust Decentralized Control Laws for the ACES Structure at the Marshall Space Flight Center, "Proceedings of the American Control Conference, May 1990 pp. 1449-1454.

[10]Allen, J. J., Lauffer, J. P., Marek, E. L., "The Sandia Structural Control Experiments," Proceedings of the First Joint U.S./Japan Conference on Adaptive Structures, Maui, HI, November 1990.

[11]Juang, J.N., Cooper, J.E., and Wright, J.R., "An Eigensystem Realization Algorithm Using Data Correlations (ERA/DC) for Modal Parameter Identification," *Journal of Control Theory and Advanced Technology*, Vol. 4, No. 1, March 1988, pp 5-14.

[12]Bendat, J.S., and Piersol, A.G., *Random Data*, Wiley-Interscience, New York, 1986.

[13]Shih, C.Y., Tsuei, Y.G., Allemang, R.J., and Brown, D.I., "Complex Mode Indication Function and its Applications," Proceedings of the 7th International Modal Analysis Conference, Las Vegas, Nevada 1989, pp. 533-540.

[14]Juang, J.N., Horta, L.G., Phan, M. Lew, J.S. Chen, C.W., "Observer/System Realization ToolBox," NASA Langley Research Center, August 21, 1991.

[15]Doyle, J. C. and Glover, K., Khargonekar, P., and Francis, B. A., "State space solutions to standard H_2 and H_∞ control problems", *IEEE* Transactions on Automatic Control, AC-34, 1989, pp. 831-847.

[16]G. J. Balas, J. C. Doyle, K. Glover, A. Packard, R. Smith, *μ-Analysis and Synthesis Toolbox (μ-Tools)*, MUSYN Inc., 1991.

[17]Steinbuch, M., Terlouw, J. C., Bosgra, O. H., "Robustness Analysis for Real and Complex Perturbations applied to an Electro-Mechanical System", *Proceedings of the 1991 Automatic Control Conference*, pp. 556.

DISTRIBUTION:

MS0899 Technical Library, 13414 (5)
MS0619 Technical Publications, 12613 (1)
MS0100 Document Processing, 7613-2(2)
For DOE/OSTI
MS9018 Central Technical Files,8523-2 (1)
MS0320 C. E. Meyers, 1011 (1)
MS0320 L. M. Lopez, 1011 (1)

MS0439 D. R. Martinez, 1434 (1)
MS0439 J. M. Redmond, 1434 (1)
MS0439 J. L. Dohner, 1434 (1)
MS0439 G. R. Eisler, 1434 (1)
MS0439 G. G. Parker, 1434 (1)
MS0501 T. G. Smith,2338 (1)
MS0501 S. M. Kohler,2338 (1)
MS0557 T. J. Baca, 2741 (1)
MS0557 J. J. Allen, 2741 (5)
MS0557 P. S. Barney, 2741 (1)
MS0557 S. E. Klenke, 2741 (1)
MS0557 J. P. Lauffer, 2741 (5)
MS0965 B. C. Brock, 9211 (1)
MS0965 M. L. Decker, 9211 (1)
MS0980 W. C. Sweatt, 9225 (1)
MS0309 A. K. Miller, 9818 (1)
MS0310 R. D. Robinett III, 9816 (1)

Mark Whorton
NASA Marshall Space Flight Center
Mail Stop ED12
MSFC, AL 35812

Alan Patterson
NASA Marshall Space Flight Center
Mail Stop ED12
MSFC, AL 35812

Angie Buckley
NASA Marshall Space Flight Center
Mail Stop PS02
MSFC, AL 35812

Dr. Henry Waites
NASA Marshall Space Flight Center
Mail Stop ED12
MSFC, AL 35812

Dr. William C. Stone
National Institute of Standards and
Technology
Bldg. 226/B168
Gaithersburg, MD 20899

Dr. D. W. Repperger
Building 33 AL/CFBS
Armstrong Laboratory
Wright Patterson Air Force Base
Dayton, Ohio 45433-6573

Professor S. S. Rao
Purdue University
School of Mechanical Engineering
West Lafayette, IN 47907

Richard S. Pappa
NASA Langley Research Center
Mail Code: 230
Hampton, VA 23665

Dr. Jer-Nan Juang
NASA Langley Research Center
Spacecraft Dynamics Branch
Mail Stop: 297
Hampton, VA 23665-5225

Dr. Robert A. Paz
Department of Electrical and Computer
Engineering
New Mexico State University
Box 30001, Dept. 3-0
Las Cruces, NM 88003-0001

Dr. N. G. Naganathan
University of Toledo
Professor of Mechanical Engineering
2801 W. Bancroft St.
Toledo, OH 43606-3390

Professor Roy R. Craig
University of Texas at Austin
ASE-EM Department
Austin, TX 78712-1085

M. G. Moeller
Harris Corporation
Government Aerospace Systems Division
P. O. Box 94000
MS 19-4737
Melbourne, FL 32902

Ray E. Gogan, Jr.
Harris Corporation
Government Aerospace Systems Division
P. O. Box 94000
Melbourne, FL 32902

Lawrence D. Davis
Harris Corporation
Government Aerospace Systems Division
P. O. Box 94000
Melbourne, FL 32902

Dr. Emmanuel Collins
Harris Corporation
Government Aerospace Systems Division
MS-32/4849
P. O. Box 94000
Melbourne, FL 32902

Dr. Young W. Kwon
Naval Postgraduate School
Department of Mechanical Engineering
Code: ME/KW
Monterey, CA 93943

Dr. Gareth Knowles
Grumman Corporate Technology
Laboratory Head
Dynamics and Control Theory
Corporate Research Center
Bethpage, NY 11714-3580

Dr. Conor Johnson
CSA Engineering, Inc.
2850 W. Bayshore Road
Palo Alto, CA 94303-3843

James R. Felty
U. S. Department of Energy
Defense Programs
DP 241 (GTN)
Washington, DC 20585

Dr. Dennis S. Bernstein
Department of Aerospace Engineering
The University of Michigan
Ann Arbor, MI 48109-2140

G. D. Althouse
Director Transportation Products
Development
Goodyear Technical Center
P. O. Box 3531
Akron, OH 4309-3531

Robert C. Schisler
Chief Engineer - Engineering Technology
Engineered Products Research Center
The Goodyear Tire & Rubber Company
1144 East Market Street
Akron, OH 4416-0001

Dr. Robert E. Skelton
Professor of Aeronautical & Astronautical
Engineering
323 Grissom Hall
W. Lafayette, IN 47907

L. Kevin Slimak
Chief Subsystems Branch
Air Force Astronautics Laboratory
AFAL/VSS
Edwards, CA 93523-5000

R. Rory Ninneman
Phillips Laboratory
PL/VTSA
Kirtland, NM 87117-6008

L. Porter Davis
Honeywell, Inc.
Satellite Systems Div.
19019 N. 59th Avenue
Glendale, AZ 85308-9650

Dr. Shalom Fisher
Naval Research Laboratory
Code 8240.1
Washington, DC 20375-5000

Charles R. Larson
Rockwell International
12214 Lakewood Boulevard
P. O. Box 7009
Mail Code: AD88
Downey, CA 90241-7009

Ben K. Wada
Jet Propulsion Laboratory
Mail Stop 157-507
4800 Oak Grove Drive
Pasadena, CA 91109

James L. Fanson
Jet Propulsion Laboratory
Mail Stop 157-316
4800 Oak Grove Drive
Pasadena, CA 91109

Dr. David C. Zimmerman
Department of Mechanical Engineering
University of Houston
Houston, TX 77204-4792

Dr. John Ware
ARC Inc.
1375 Piccard Drive
Rockville, MD 20850

Dr. Gonzalo J. Rey
Moog Inc., Technology Center
East Aurora, New York 14052-0018

Dr. Vittal S. Rao
Director, Intelligent Systems LCenter
University of Missouri-Rolla
321 Engineering Research Laboratory
Rolla, MO 65401-0249

Capt. Gregory S. Agnes
Wright Laboratory
WL/FIBGC
WPAFB, OH 45433

Dr. John Breakwell
Lockheed Missiles & Space Company
P. O. Box 3504
Sunnyvale, CA 94088-3504

Dr. G. E. Young
School of Mechanical and Aerospace
Engineering
Oklahoma State University
Stillwater, OK 74078